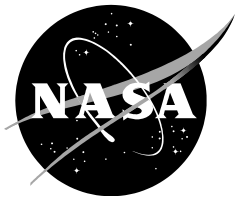# Changes in Flat Plate Wake Characteristics Obtained with Decreasing Plate Thickness

Man Mohan Rai
Ames Research Center
Moffett Field, CA-94035

July 2016

NASA STI Program ... in Profile

Since its founding, NASA has been dedicated to the advancement of aeronautics and space science. The NASA scientific and technical information (STI) program plays a key part in helping NASA maintain this important role.

The NASA STI program operates under the auspices of the Agency Chief Information Officer. It collects, organizes, provides for archiving, and disseminates NASA's STI. The NASA STI program provides access to the NTRS Registered and its public interface, the NASA Technical Reports Server, thus providing one of the largest collections of aeronautical and space science STI in the world. Results are published in both non-NASA channels and by NASA in the NASA STI Report Series, which includes the following report types:

- TECHNICAL PUBLICATION. Reports of completed research or a major significant phase of research that present the results of NASA Programs and include extensive data or theoretical analysis. Includes compila-tions of significant scientific and technical data and information deemed to be of continuing reference value. NASA counter-part of peer-reviewed formal professional papers but has less stringent limitations on manuscript length and extent of graphic presentations.

- TECHNICAL MEMORANDUM. Scientific and technical findings that are preliminary or of specialized interest, e.g., quick release reports, working papers, and bibliographies that contain minimal annotation. Does not contain extensive analysis.

- CONTRACTOR REPORT. Scientific and technical findings by NASA-sponsored contractors and grantees.

- CONFERENCE PUBLICATION. Collected papers from scientific and technical conferences, symposia, seminars, or other meetings sponsored or co-sponsored by NASA.

- SPECIAL PUBLICATION. Scientific, technical, or historical information from NASA programs, projects, and missions, often concerned with subjects having substantial public interest.

- TECHNICAL TRANSLATION. English-language translations of foreign scientific and technical material pertinent to NASA's mission.

Specialized services also include organizing and publishing research results, distributing specialized research announcements and feeds, providing information desk and personal search support, and enabling data exchange services.

For more information about the NASA STI program, see the following:

- Access the NASA STI program home page at http://www.sti.nasa.gov

- E-mail your question to help@sti.nasa.gov

- Phone the NASA STI Information Desk at 757-864-9658

- Write to:
  NASA STI Information Desk
  Mail Stop 148
  NASA Langley Research Center
  Hampton, VA 23681-2199

NASA/TM-2016-219142
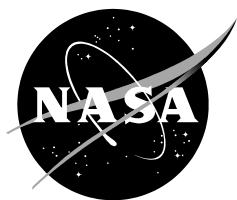
Changes in Flat Plate Wake Characteristics Obtained with Decreasing Plate Thickness

Man Mohan Rai
Ames Research Center
Moffett Field, California

July 2016

CHANGES IN FLAT PLATE WAKE CHARACTERISTICS OBTAINED WITH DECREASING PLATE THICKNESS

Man Mohan Rai[1]
NASA Ames Research Center, Moffett Field, CA-94035

ABSTRACT

The near and very near wake of a flat plate with a circular trailing edge is investigated with data from direct numerical simulations. Computations were performed for four different Reynolds numbers based on plate thickness (D) and at constant plate length. The value of θ/D varies by a factor of approximately 20 in the computations (θ being the boundary layer momentum thickness at the trailing edge). The separating boundary layers are turbulent in all the cases. One objective of the study is to understand the changes in wake characteristics as the plate thickness is reduced (increasing θ/D). Vortex shedding is vigorous in the low θ/D cases with a substantial decrease in shedding intensity in the largest θ/D case (for all practical purposes shedding becomes almost intermittent). Other characteristics that are significantly altered with increasing θ/D are the roll-up of the detached shear layers and the magnitude of fluctuations in shedding period. These effects are explored in depth. The effects of changing θ/D on the distributions of the time-averaged, near-wake velocity statistics are discussed.

INTRODUCTION

The wake of the thin flat plate with turbulent boundary layers and a sharp trailing edge has been discussed in numerous articles, one of the earliest being that of Chevray & Kovasznay (1969). The ratio of the boundary layer momentum thickness to the trailing edge thickness of the plate (θ/D) is large (23.2) in their study. Profiles of measured mean velocity and turbulent normal intensities and shear stress are provided. The boundary layers in this study merge slowly to form the wake and vortex shedding is absent.

Ramaprian et al (1982), based on their own experimental data for a flat plate with a sharp trailing edge and, data from other investigations conclude that the wake only reaches an asymptotic state for x/ **θ** > 350 (**θ** is the momentum thickness of the *wake* in their study); they refer to the wake region upstream of this location as the "developing wake". The developmental region is further divided into the near wake (x/**θ** < 25) and intermediate wake (25 < x/**θ** < 350). The near wake experiences the development of an inner wake and is influenced by the wall-layer of the upstream boundary layers. In the intermediate wake the effect of the upstream boundary layer diminishes and ultimately becomes insignificant.

Nakayama & Liu (1990) investigate the potential Reynolds number dependence of the wake centerline velocity profiles (normalized by the wall variables at the trailing edge), indicated by earlier experimental data. Their experiments (low Reynolds number, sharp trailing edge) show that indeed the profiles are Reynolds number dependent, with higher profiles obtained at higher Reynolds numbers. They conjecture that this is because of the effect of outer-layer eddies on the spreading of the inner wake.

Hayakawa & Iida (1992) have obtained flat plate wake data with a fine trailing edge (0.2mm) to better investigate the very near wake ($x^+ < 500$). The centerline velocity was found to recover in a manner similar to the turbulent boundary layer. The peak values in normal intensities and shear stress profiles in

---

the cross-stream direction were found to first increase from that obtained at the trailing edge before diminishing further downstream. Based on space-time correlations, the authors attribute the initial increase in intensities and shear stress to an interaction between the wall turbulence on either side of the plate upon traveling past the trailing edge and a consequent change in orientation of longitudinal vortices. Of interest is the appearance of a broadband peak in cross-stream velocity spectra with increasing x, indicating quasi-periodicity (possibly due to vortices or wave-like motions).

In addition to the experimental investigations mentioned above analytical solutions based on certain simplifying assumptions are provided by Albers (1980). In essence, the centerline velocity distribution in the near wake can be approximated by a logarithmic relation similar in form to that obtained for the turbulent boundary layer upstream of the wake in these cases. A good comparison is obtained between experimental data and the wake 'log-law' in the near wake.

Thomas & Liu (2004) report on an experimental investigation of symmetric and asymmetric turbulent wakes behind a flat plate. The thickness of the plate is tapered down to 1.6 mm at a taper angle of 2.2^o in the last 0.2 meters of the plate length. Hence, as in earlier flat plate wake experiments, little or no shedding is expected. The asymmetric wake is obtained by introducing a semicircular bump on the lower side and a suction slot on the upper side. The net effect is a ratio of θ_L/θ_U of 2.5. Data are provided for adverse, favorable and zero pressure-gradient wakes.

In contrast to the thin plate with a sharp trailing edge, the thick plate with a blunt trailing edge (small θ/D cases), exhibits vigorous vortex shedding. Unlike the case of the cylinder, the Reynolds number based on momentum thickness of the boundary layer at the trailing edge (Re_θ) and the Reynolds number defined using the thickness of the flat plate **or** the diameter of its trailing edge (Re_D), are independent parameters. A detailed investigation of the wake of the thick plate with a circular trailing edge and, *turbulent separating boundary layers,* was initiated by Rai (2013, 2014 & 2015). This was accomplished with the aid of direct numerical simulations (DNS). The boundary layers as well as the wake were computed via DNS in these investigations. The separating boundary layers are fully turbulent well upstream of the trailing edge and are statistically identical. Thus the wake is symmetric in the mean.

In Rai (2013) distributions of the phase-averaged turbulent intensity and shear stress (random component) in the near wake are explored and compared with cylinder experimental data. Wherever possible a physical explanation of the origin of the important features of the distributions, as well as one based on the distribution of the production term in the corresponding budget, is provided. A new event-based phase-averaging procedure is introduced. A first effort at visualizing some of the important features of the near wake, such as the strength and structure of rib vortices in relation to the shed vortices, their evolution in time, the internal structure of shed vortices etc. are provided here. Some of the findings are as expected (rib vortices in the braids) while others such as the presence of intense elongated spanwise vortices and the absence of a single columnar vortex in the cores provide new understanding of the cores and braids and the interaction between them. Earlier research had primarily dealt with rib vortices as they occur in the braid and the amplification of the streamwise and transverse vorticity associated with them by vortex stretching as a result of the associated strain rate. In Rai (2013), it is found, that on average the stretching of rib vortices via the phase-averaged strain rate produces significantly less turbulent vorticity than that produced by turbulent stretching both in the braids and in the cores. In particular the data show the importance of turbulent stretching in sustaining fluctuations in the spanwise component of vorticity.

In Rai (2014) the emphasis is on the stability of the detached shear layers, rib-vortex induced reverse flow, and phase-averaged distributions of the random component of normal intensities and shear stress and the production term in the corresponding budgets in the *very* near wake (x/D < 3.0). It was determined that, as in the case of the cylinder with laminar separating boundary layers, the flat plate wake also exhibits shear layer instability followed by the formation of shear layer vortices that have a profound impact on the structure of the shear layer and the formation of the shed vortices. However, unlike the cylinder cases, here only a small fraction of the separated turbulent boundary layer participates in the

initial formation of the shed vortices and, it is this fraction that is unstable. As in Rai (2010) (cylinder case), periods of shear layer instability correlated well with the interaction of the shear layer with recirculation region vortices, and quiescent periods showed little or no interaction between the two. This is a strong indicator that this interaction is an important contributor to the initiation of the instability. Spectra of the time-varying velocity and pressure within the shear layers at x/D = 0.5 were obtained. Unlike the cylinder case with laminar separating boundary layers, the spectrum of streamwise velocity did not show a broadband peak. This is because of the large velocity fluctuations that are already present in the detached shear layer at its inception (turbulent separating boundary layer). The pressure signal on the other hand showed a clear broadband peak with the characteristic shear layer frequency.

An examination of the distribution of streamwise velocity in the wake center-plane (Rai, 2014) first led to the discovery of regions of isolated reverse flow that are disconnected from the main body of reverse flow in the trailing edge region. They are first formed near the trailing edge and convect downstream. These regions are a result of powerful rib vortices that are formed in the high-strain-rate region that exists between the shed vortices in their initial state; they are quite energetic with streamwise velocities (negative) within them reaching 40% of the freestream velocity. They are accompanied by pressure minima and relatively high cross-stream vorticity levels and are observed as far downstream as x/D = 4.0. These reverse flow regions occur at multiple spanwise (z) locations within short periods (25% of shedding period); thus they appear along nearly constant time lines in a (t, z) plane at a given x location in the wake center-plane. Two such lines of reverse flow (each line corresponding to the passage of a shed vortex) are observed per shedding period. A spectral analysis of the z-averaged negative streamwise velocity shows a peak at twice the shedding frequency thus confirming the frequency of occurrence of these lines of multiple reverse flow regions. The passage of the shed vortices over a given x location reduces the local streamwise velocity near the center-plane thus creating favorable conditions for rib-vortex induced reverse flow. Since all such regions of isolated reverse flow investigated showed an associated rib vortex, it was concluded that the rib vortices were the causative agent. These regions eventually weaken and disappear; probable reasons being a re-orientation of the rib vortices (lowering of cross-stream vorticity) and the increase in streamwise velocity with increasing x.

In Rai (2015) the emphasis is on entrainment and the instability of the detached shear layers. It was observed in Rai (2014) that only a small fraction of the separating turbulent boundary layer forms the detached shear layer and participates in the initial roll-up into the shed vortex. A natural consequence of this behavior is that for some distance downstream the wake with its shed vortices ingests fluid that was originally part of the turbulent boundary layer. The log-layer eddies are assimilated in this process and become a part of the shed vortices or the braids. A visualization of this process is provided in the article. A visualization of the effect of increasing θ/D on assimilation/entrainment is also provided; it clearly shows that wakes with larger θ/D values continue to assimilate boundary layer fluid for longer (until a larger value of x/D). The study (Rai, 2015) also shows that wake cross-stream TKE profiles, in the region away from the shed vortices and braids, are very close to that of the upstream turbulent boundary layer (especially in the very near wake for the large θ/D cases). This again is a consequence of the fact that much of the turbulent boundary layer does not participate in the initial shed-vortex roll-up process.

A visualization of shear-layer instability events in a (t, z) plane in Rai (2015) showed that shear-layer vortex generation rates can vary as much as a factor of two from event to event. An analysis of velocity fluctuations in the upstream boundary layer indicated that high-speed streaks near the trailing edge result in higher shear-layer vortex generation rates.

The findings of Rai (2014) strongly indicate that a primary cause of the shear-layer instability is the interaction between the shear layer and recirculation region vortices. This of course raises the question, do the disturbances within the shear layer (originating in the boundary layer upstream) and the log-layer eddies (that convect past the trailing edge) play a role in generating shear-layer vortices as well? The investigation of Rai (2015) shows that log-layer eddies, like recirculation region vortices, can

generate shear-layer vortices. However, because log-layer eddies are convected at a relatively high rate, they usually produce only one shear-layer vortex and continue to interact with it during their passage over the shear layer. Recirculation region vortices, on the other hand, remain in approximately the same position relative to the shear layer because of the much lower convections rates that they encounter. Thus they tend to produce a few shear-layer vortices that can be relatively powerful.

The objective of the present investigation is to better understand the changes in the characteristics of the wake of a flat plate with a circular trailing edge and turbulent separating boundary layers (in particular changes in shedding and related wake features), as the plate becomes very thin in relation to the boundary layer thickness (increasing θ/D). Changes in, for example, the coherence of the shed vortices (in the spanwise direction), roll-up of the detached shear layers, centerline velocity spectra, time-averaged velocity statistics and the basic shedding mechanism (initiation of circulation) are all topics of interest and are discussed in this article. Some of the reasons underlying the substantial changes in the observed flow features as θ/D is increased, are also provided. The data used in the present investigation are obtained from direct numerical simulations of flat plate flow for four different values of Re_D (at constant plate length). The turbulent boundary layers and the wake are all computed via DNS. Here we continue the analysis of the near wake of the flat plate initiated in Rai (2013, 2014 & 2015).

Although of interest, an investigation of base pressure variation is not included in the present article. The investigations of Buresti et al (1997, the effect of rounding a rectangular trailing edge on drag) and Rowe et al (2001, the effect of boundary layer thickness on base pressure) and the references cited therein provide an introduction to the topic.

Cylinder Vortex Shedding

Prior to embarking on the very complex shedding process that occurs in the case of flat plates with turbulent separating boundary layers, it seems appropriate to examine vortex shedding in the case of cylinders at low Reynolds numbers. Accordingly, a computation of cylinder flow at $Re_D = 195$ was performed on the grid utilized in Rai (2010) for the Case $Re_D = 3900$. The computational method used is the same as in Rai (2010). The results presented below were obtained after the initial transients had subsided and a time-periodic flow was established. We start with the following questions: What are the events that result in the *initial region of circulating flow and associated center* during shedding? What role does the velocity field induced by the previously shed vortex (or two) play in the formation of the subsequent shed vortex? Does the shear-layer play a role? Does the initial circulating flow and the shear-layer roll-up occur simultaneously? Does the associated minimum in pressure appear at the same time as the initial circulating flow or later? The answers are provided below.

In the following figures the focus is on three different phases, ϕ_A (prior to appearance of circulating flow), ϕ_B (soon after the appearance of circulating flow), and ϕ_C (soon after the appearance of the associated pressure minimum), $\phi_A < \phi_B < \phi_C$. Figure 1a shows instantaneous velocity vectors, and pressure contours showing the pressure minimum associated with the relatively well-formed upper vortex (clockwise rotation) at the phase ϕ_A. The flow in the region below the centerline is largely downward with the area near the base showing flow towards the base that then curves sharply and subsequently points downstream. Figure 1b is an enlarged view of the region within the rectangle in Fig. 1a; it confirms the observation that circulating flow is not observed at this phase. The downward flow very near the base is a remnant of the flow induced by the previous *positive shed vortex*. Further away from the base the downward flow is induced by the upper negative vortex and also the previously shed positive vortex.

Figures 2a and 2b are the counterparts of Figs 1a and 1b, but at the phase ϕ_B. Here the first signs of circulating flow are seen within the rectangle in Fig. 2a. This circulatory flow is clearly visible in Fig. 2b. The question that arises then is, what causes the flow to circulate and exhibit a center? Very close to the base (in the vicinity of the red arrow) we continue to observe downward flow caused by the previous positive shed vortex. Comparing the pressure contours in Figs. 1a & 2a, it is clear that the upper negative

vortex has moved to the right and downward with increasing phase. The downward movement of this vortex causes it to have a greater influence on the flow below the centerline. This movement causes the flow near the base and below the centerline to turn upward and to the left.
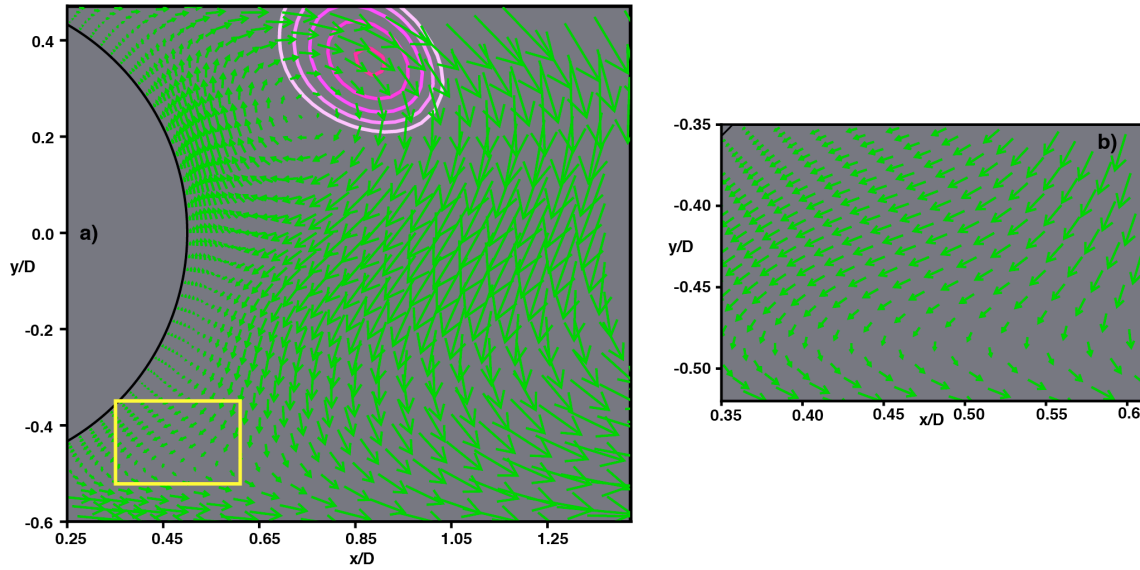

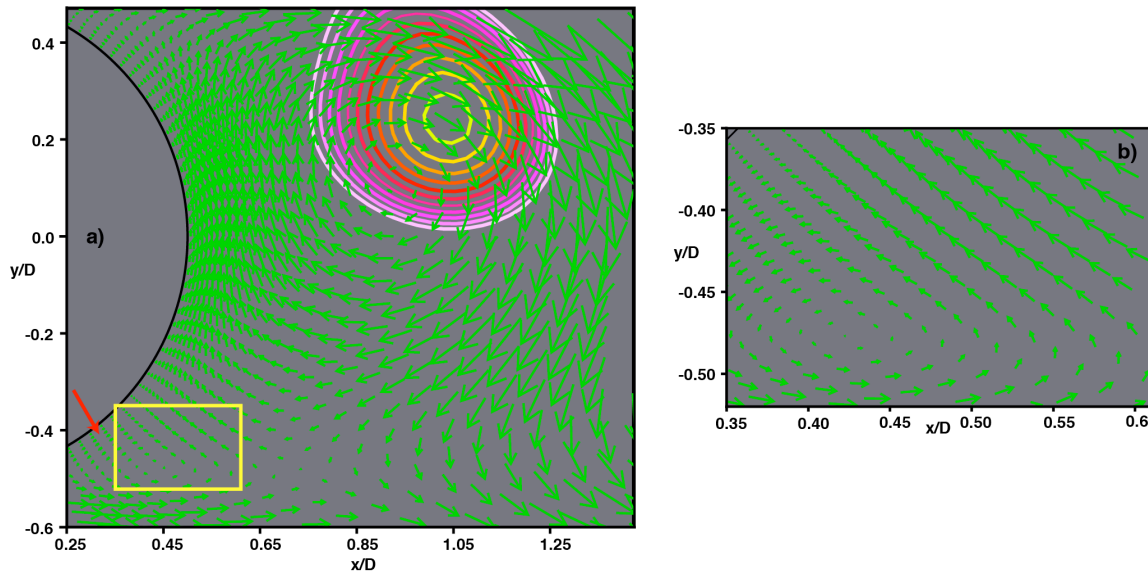Figure 1. Velocity vectors and pressure contours for the cylinder at $\phi = \phi_A$.

Figure 2. Velocity vectors and pressure contours for the cylinder at $\phi = \phi_B$.

The flow in the lower shear layer, and even further below, continues to point in the positive x direction. Clearly, the necessary constituents for circulatory flow are present at this phase: downward flow very near the base, reverse flow below the centerline and forward flow in the shear layer. The upward motion caused by the upper vortex (left of its center) causes the shear layer flow also to turn slightly upward. The end result is circulating flow very near the base and a saddle point to its right. *Thus, the flow induced by the two previous shed vortices (negative/positive) together with the forward flow in the shear layer, are directly responsible for the initiation of circulating flow.* A contour plot of instantaneous pressure with a large number of contours did not show any evidence, or tendency toward, an associated minimum in pressure at the phase ϕ_B. The lower detached shear layer, as visualized by spanwise vorticity contours

(not shown here), does not roll-up at this phase. *Thus the initially observed circulating flow is a direct result of the two previously shed vortices and, it precedes the appearance of the pressure minimum and the roll-up of the shear layer.* Shear-layer roll-up and the circulating flow (associated with the vortex) are sometimes thought of as two simultaneously occurring attributes of the same phenomenon. Instead, the circulatory flow associated with the newly formed vortex and the previously shed vortex results in a redistribution of the shear-layer spanwise vorticity that results in the shear layer roll-up.

Figures 3a and 3b are also counterparts of Figs. 1a and 1b, but at the phase ϕ_C. The circulatory flow is evident. However, instantaneous pressure contours at this phase show a minimum (marked with an x in Fig. 3a and with both an x and pressure contours in Fig. 3b). The center of rotation and the pressure minimum are at slightly different locations. Subtracting the velocity at the pressure minimum from the velocity field and redrawing the velocity vectors (being in a frame of reference moving with the velocity at the pressure minimum) moves the center to the pressure minimum but little else. At later phases the center and pressure minimum move to the right, the shear-layer shows a distinct roll-up and the new vortex strengthens. With this understanding of the initial vortex formation process in a relatively simple case, it remains to be seen if the flat plate with turbulent separating boundary layers also exhibits similar shedding characteristics and if these characteristics persist as θ/D is increased considerably.
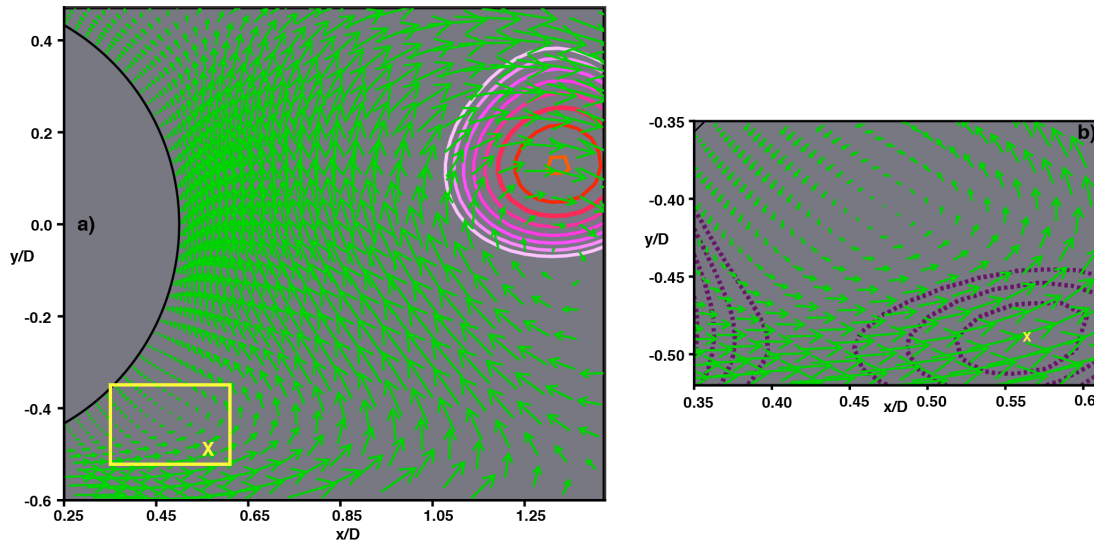

Figure 3. Velocity vectors and pressure contours for the cylinder at $\phi = \phi_C$.

PLATE COMPUTATIONAL GRID, FLOW/GEOMETRY PARAMETERS AND NUMERICAL METHOD

The computational region for the flat plate DNSs is divided into two zones to facilitate grid generation and provide adequate grid resolution for the wake. Figure 4 shows the plate cross-section and the two zones that comprise the computational region. The three-dimensional zones and grids are obtained by uniformly spacing copies of these two-dimensional zones in the spanwise direction (*z*). The plate zone is bounded by four boundaries: the plate surface (excluding the trailing edge), an external boundary and, two zonal boundaries (top and bottom) that interface with the wake zone. The plate zone captures the flow-field upstream of the trailing edge including the plate boundary layers. The leading edge of the plate is an ellipse. The wake zone is constructed to provide adequate grid resolution for the detached shear layers, the recirculation region and the wake. The boundaries of this zone include the circular trailing edge, the upper and lower boundaries and the exit boundary. Both the upper and lower boundaries consist of a zonal boundary segment that interfaces with the plate zone and a second segment that serves as an external boundary. Direct numerical simulations for four different values of Re_D were performed to obtain the data used in this study (Cases A, D, E & F). Of these, only Cases E & F were computed as a part of the current effort.

The placement of the various boundaries in relation to the plate surface in Cases A & D is provided in Rai (2013, 2014 & 2015). The vertical extent of the wake zone near the trailing edge, where its upper/lower boundaries are horizontal is large enough to completely contain the wake in all cases (Fig. 4 in Rai 2013 clearly shows the adequacy of this dimension in Case A). The spanwise extent of the region in Cases A & D is 4.0D. *Cases A & D of the present study are labeled as A & D in Rai (2015) as well.*
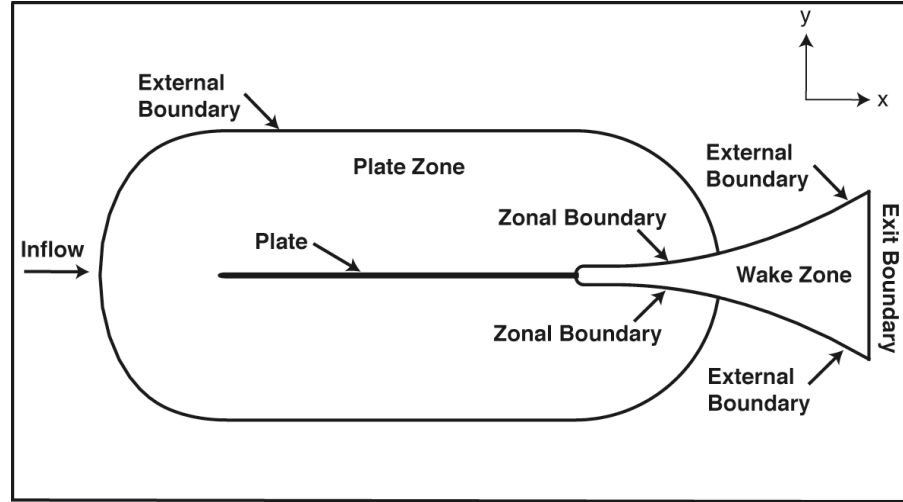

Figure 4. Midspan plate section and multiple zone discretization of the computational region (Rai 2013).

Figure 5 shows representative grids in the vicinity of the trailing edge in both zones. These grids were generated with an algebraic grid generator. Both the grids have the same spacing in the wall normal direction at the plate surface. The grid in the wake zone transitions from curvilinear near the trailing edge to rectangular downstream. In Cases A & D, downstream of x/D ≈ 13.5, the wake grid coarsens gradually in the x direction. In addition to reducing the computational costs, this coarsening dissipates the wake to a degree that inviscid exit boundary conditions can be employed at the exit boundary of the wake zone.
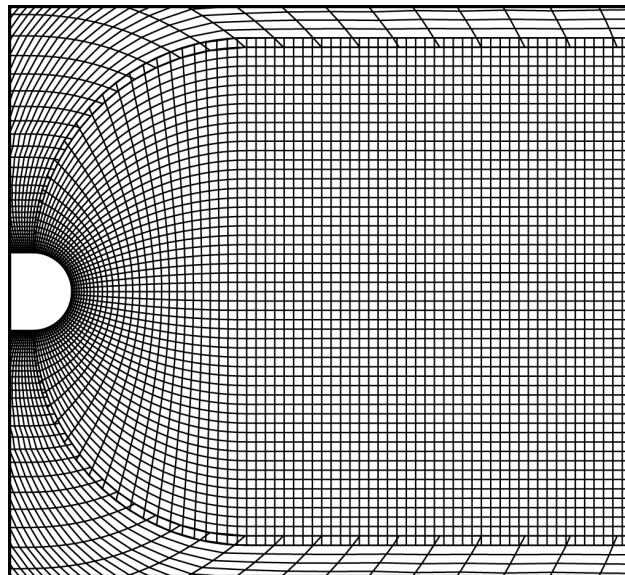

Figure 5. Representative grids in the plate and wake zones in the trailing edge region (Rai 2013).

The wake grid for Case A was constructed with 741 grid points in the streamwise direction, 411 in the cross-stream direction and 256 in the spanwise direction (about 78 x 10^6 grid points). The resolution achieved along the centerline in the three spatial directions at x/D = 10.0 is approximately $\Delta x/\eta$ = 3.7, $\Delta y/\eta$ = 2.2 and $\Delta z/\eta$ = 2.1 where η is the computed Kolmogorov length scale at the same location. The grid resolution in the plate grid in the x, y and z directions for this case is about 17.8, 0.84 and 6.6 wall units respectively, based on the wall shear velocity near the end of the plate. The resolution achieved in all four cases used here is similar. The adequacy of the grid resolution and domain size used is demonstrated in Rai (2013 & 2014). A comparison of computed boundary layer turbulent intensities with experimental data is provided in Rai (2013). The computations are performed at a Mach number of 0.2.

The primary goal in the current investigation is to study the effect of substantially increasing θ/D on various characteristics of the wake. Accordingly, the thickness of the plate in Cases E and F was reduced by a factor of 2 & 8, respectively, from that used in Case D. The length of the plate in Cases E & F was the same as in Cases A & D. In Cases E and F the *physical extent* of the computational region in the z direction (Δz) was kept the same as in Case D to ensure that the computed statistics on the plate were not affected by the imposition of periodicity in the z direction. However, the thickness of the plate was reduced as mentioned earlier. This resulted in the spanwise (z) extent of the computational region being 8.0D and 32.0D in Cases E & F, respectively. The grid resolution in the z direction, however, is the same as in Case D. For the same reason (an accurate simulation/representation of the separating boundary layer), the vertical extent (physical) of the wake region (in the region where the upper and lower boundaries are horizontal) was also maintained at approximately the same value as in Case D; the grid resolution is approximately the same. The same reasoning was also used in the placement of the external boundary of the plate zone and the exit boundary of the wake zone in Cases E & F (in terms of the plate thickness they were placed approximately 2 and 8 times further away compared to Case D). The grid spacing in the wall-normal direction in Cases E & F is half that used in Cases A & D to better resolve the smaller trailing edges. Values of Re_D and the ratio $\psi = (\theta/D)/(\theta/D)_{Case\ A}$ for the different cases are provided in Table 1. The ratio ψ is essential in comparing the value of (θ/D) for any given case to that of the reference case (Case A); it varies substantially over the cases considered (by a factor of 20.43). The Reynolds number based on plate length L is the same in all cases, Re_L = 1,255,000.

	Re_D	ψ
Case A	10,000	1.00
Case D	5000	2.28
Case E	2500	4.89
Case F	625	20.43

Table 1. Re_D and ψ for Cases A, D, E & F.

A high-order accurate upwind-biased method is used here to compute the flow over the plate as well as that in the wake. The convective terms are computed using sixth- and seventh-order upwind-biased finite differences, both with seventh-order dissipation terms. The viscous terms are computed with fourth-order central differences. The method is iterative-implicit in nature, multiple iterations are employed at each time-step to solve the nonlinear finite-difference equations arising from a fully implicit formulation; the method is second-order accurate in time. The boundaries that contain the computational grids can be classified as natural and zonal boundaries. The natural boundaries include the external boundary of the plate grid, the surface of the plate, the exit boundary of the wake grid, the segments of the upper and lower boundaries of the wake grid labeled as "external boundary" in Fig. 4, and, the boundaries in the *z* direction. The upstream segment of the upper boundary between the plate and wake grids is an example of the zonal boundaries used in the computation. Periodic boundary conditions are imposed on the boundaries in the *z* direction (homogeneity in *z*). No-slip/adiabatic wall conditions are used on the plate surface. Wall blowing/suction is implemented on a short segment on both the upper and lower surfaces of the plate to induce transition to turbulence. The boundary layer is turbulent well upstream of the trailing edge. The upper and lower transitional/turbulent boundary layers and the wake are all computed via DNS.

The natural and zonal boundary conditions, and the high-order accurate upwind-biased finite-difference method used here are discussed in brief in Rai (2015) and in detail in the articles cited therein.

RESULTS

The data provided in the following figures were obtained during the data-sampling period (after the initial transients were eliminated). The time-step $n = 0$ corresponds to the time at which sampling was initiated. In the following contour plots the colors blue/green represent negative values (deep blue representing the lowest value) of the term/quantity being discussed. Orange, red and magenta represent positive values (magenta bordering on white representing the highest value). Shades of yellow represent values close to zero. The approach taken here is to use the test case (A, D, E or F) that highlights the attribute that is being discussed, followed as necessary by appropriate remarks regarding the same attribute as it appears in the remaining cases. Velocity statistics etc. were obtained over 160 shedding periods for Case A, 200 shedding periods for Case D, 180 for Case E and 430 for Case F. The time-step used in cases A & D is approximately $U\Delta\tau/D = 0.0033$; this corresponds to about 1750 time steps per shedding period in Case A. The time step used in cases E and F is half as much (the grid spacing at the wall in the wall-normal direction for these two cases is half that used in Cases A & D).

Vortex shedding in Cases A, D & E

We begin the investigation of shed vortex structure, and the manner in which it changes with increasing (θ/D), in Cases A, D & E with a top view of surfaces of constant pressure (Fig. 6).
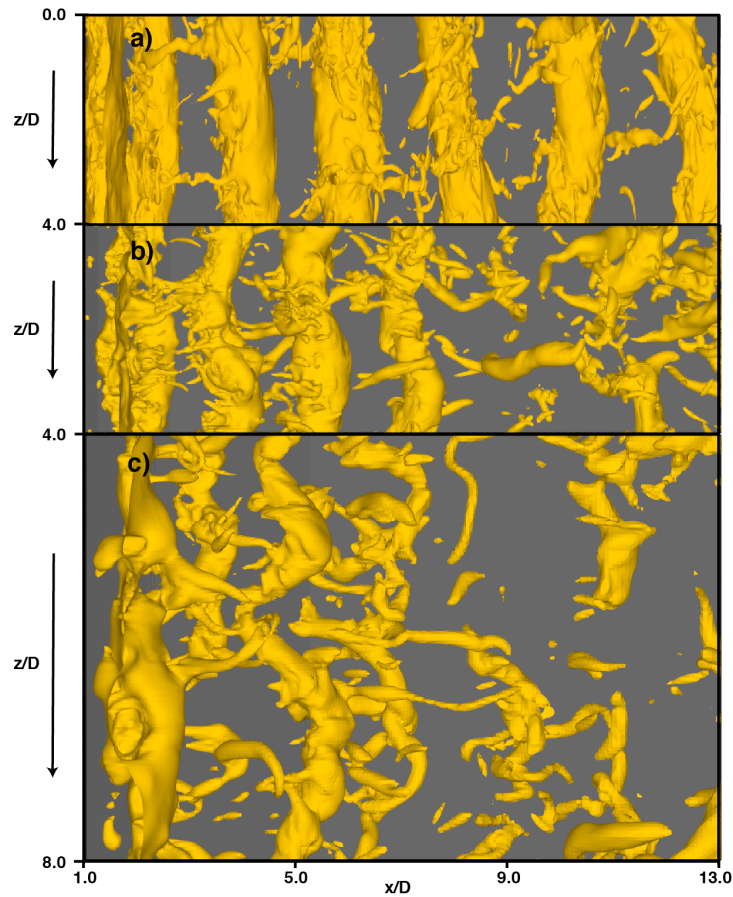

Figure 6. Instantaneous surfaces of constant pressure (top-view), a) Case A ($\psi = 1.00$, n = 70000), b) Case D ($\psi = 2.28$, n = 180,000), c) Case E ($\psi = 4.89$, n = 192,000).

Figure 6a shows an instantaneous constant pressure surface for Case A. The shed vortices are clearly observed as nearly cylindrical regions of low pressure. They show little distortion in the z direction. The rib vortices in the braid regions connecting consecutive shed vortices of opposite sign are also evident as narrow tubes; some of them are highly distorted. Shed vortices that are ruptured or that show large distortions are rare in Case A (one ruptured vortex was identified and reported in Rai (2013) for Case A). Figure 6b shows an instantaneous constant pressure surface for Case D. The larger spanwise distortions near the base region (in comparison to Case A) and what appears to be the beginning of vortex breakdown further downstream is evident (less structured shedding as θ/D increases by a factor of 2.28). Because it is tempting to consider this loss in coherency as solely due to vortex breakdown processes, we hasten to add that the complexity in vortex structure is sometimes evident at shed vortex inception very near the trailing edge. *This is an indication that, at times, the formation process itself varies considerably from the norm.* The underlying reasons will become evident in the figures that follow.

Case E (Fig. 6c, which involves a further increase of θ/D) yields significant vortex distortion in the entire near-wake region. Obtaining phase-averaged statistics in this case is difficult because of this distortion and reasons relating to cross-sectional structure of the shed vortices. It is clear from Figs. 6a – 6c that increasing θ/D beyond a certain level results in the loss of coherence of shed vortices. The spanwise extent of the computational region in Case E is 8.0D whereas in Case D it is 4.0D although the actual physical extent in the z direction is the same in these two cases.

The loss in coherence of the shed vortices with increasing θ/D has an effect on the induced cross-stream velocity (v) at the wake center-plane (y/D = 0.0). Figures 7a and 7b show contours of instantaneous v for Cases A and D respectively, at the same time instants as in Figs. 6a and 6b, in the wake center-plane. Figure 7a shows bands of positive and negative v, caused by the passage of successive shed vortices, that are nearly vertical but with considerable small-scale structure. In Fig. 7b the band structure begins to show waviness in the z direction and incursions of positive regions into negative bands and vice versa past the location x/D ≈ 7 (Case D).
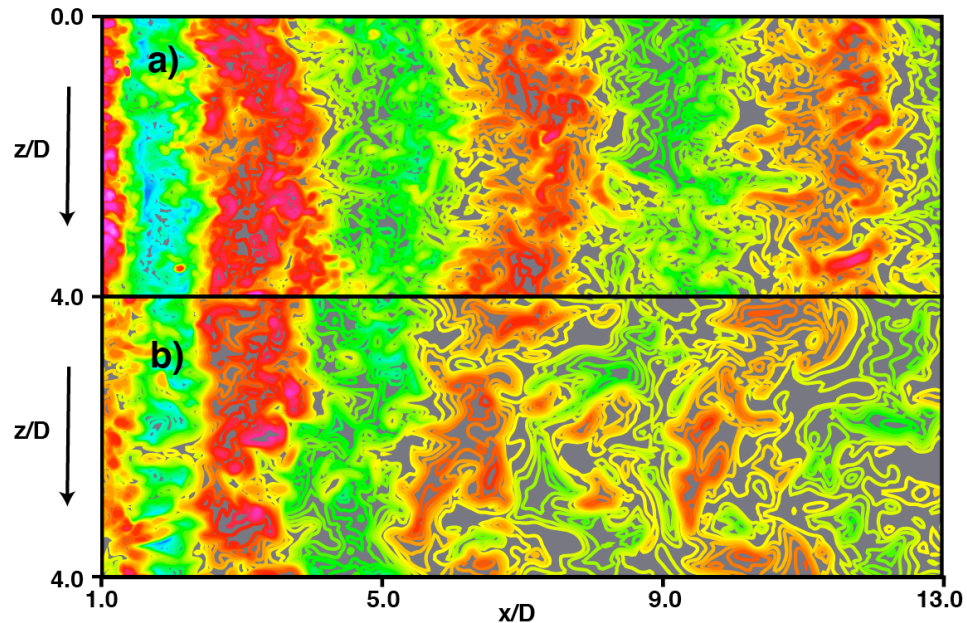
Figures 7. Instantaneous contours of v in the wake center-plane, a) Case A (ψ = 1.00, n = 70000), b) Case D (ψ = 2.28, n = 180,000).

Contours of instantaneous spanwise vorticity in an (x, y) plane for Cases A and E are shown in Figs. 8a and 8b, respectively; they are provided to better understand the loss in coherence with

increasing θ/D. As mentioned in Rai (2014), the shed vortex at inception (in this instance the lower one) is not a single cylindrical vortex as in low Reynolds number cylinder flows. Instead, it is an amalgam of several smaller vortices of both signs. Vortices of the same sign as the vorticity in the shear layer that is rolling up are dominant. In addition, segments of the shear layer and shear-layer vortices are incorporated in the newly forming vortex. The region where the contours are clustered does not include the log-layer. The log-layer eddies convect past the trailing edge and may then be assimilated by the shed vortices (for sufficiently small values of θ/D). These attributes are evident in Fig. 8a (Case A). Figure 8b shows instantaneous spanwise vorticity contours for Case E. The differences between Figs. 8a and 8b are striking. Firstly, relative to the thickness of the plate, the thickness of the detached shear layers in Case E is considerably larger than in Case A. Secondly, much of the small-scale activity seen in Fig. 8a is absent in Fig. 8b.
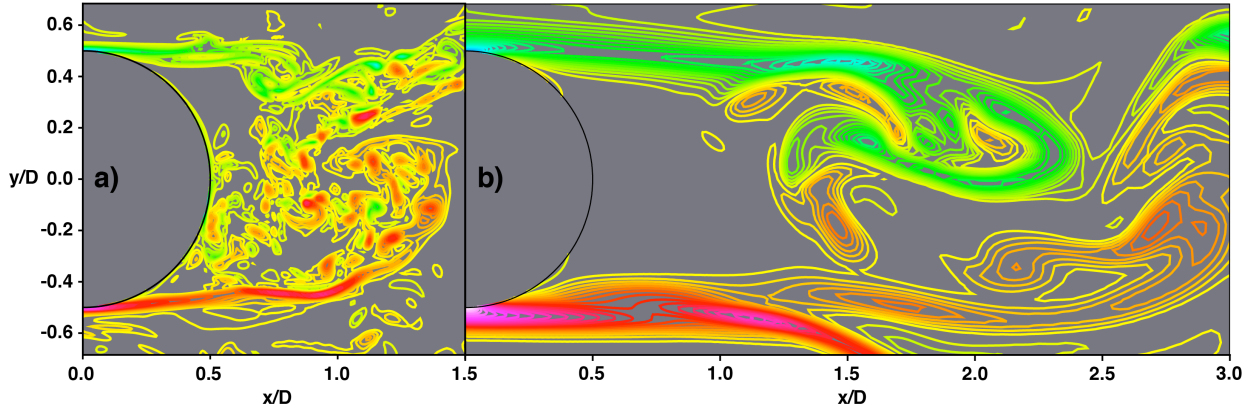
Fig. 8. Instantaneous contours of spanwise vorticity in an (x, y) plane, a) Case A (ψ = 1.00, n = 470, z/D = 0.0) and b) Case E (ψ = 4.89, n = 2560, z/D = 0.0).

The third and perhaps the most important difference is that the two detached shear layers (DSLs) in Fig. 8b are separated by a physical distance that is approximately one quarter of that in Fig. 8a (the trailing edge diameter in Case E is 0.25 times that in Case A). The smaller separation results in a stronger interaction between the DSLs in Case E. There is less room for a more conventional, approximately circular, roll-up of the DSLs as in Case A. Instead, often a folding of the DSL into two distinct layers occurs as in Fig. 8b. The resulting shed vortex is initially stretched out in the x direction and sometimes breaks up into multiple shed vortices that occasionally reconstitute into a single larger shed vortex. The end result is the lack of coherence seen in Fig. 6c.

Figures 9a and 9b show contours of instantaneous spanwise vorticity at a given instant but at z/D = 0.0 and at z/D = 4.0 (midspan) for Case E. The primary positive vortex occurs at approximately x/D = 2.0 in Fig. 9a but at x/D = 2.7 in Figure 9b (see arrows). At x/D = 2.7 in Fig. 9a we only have a relatively quiescent shear layer. Figures 9a and 9b once again show the lack of coherence in the z direction and also that, occasionally the shed vortices, even in Case E, are approximately circular.

Contours of time-averaged spanwise vorticity for cases A and E are provided in Figs.10a and 10b, respectively. These figures clearly show the much larger separation between the upper and lower shear layers in Case A compared to that obtained in Case E. The proximity of the two shear layers can be expected to have a significant effect on the shed vortex formation process. This effect of decreasing separation distance will become more apparent in Case F that is discussed in the next section. A second feature of interest in Fig. 10 is the streamwise extent of the high vorticity region; it is about twice as much in Case E, in terms of the diameter D, as in Case A. The minimum and maximum values of spanwise vorticity and the number of contours specified in obtaining Figures 8, 9 & 10 are identical.
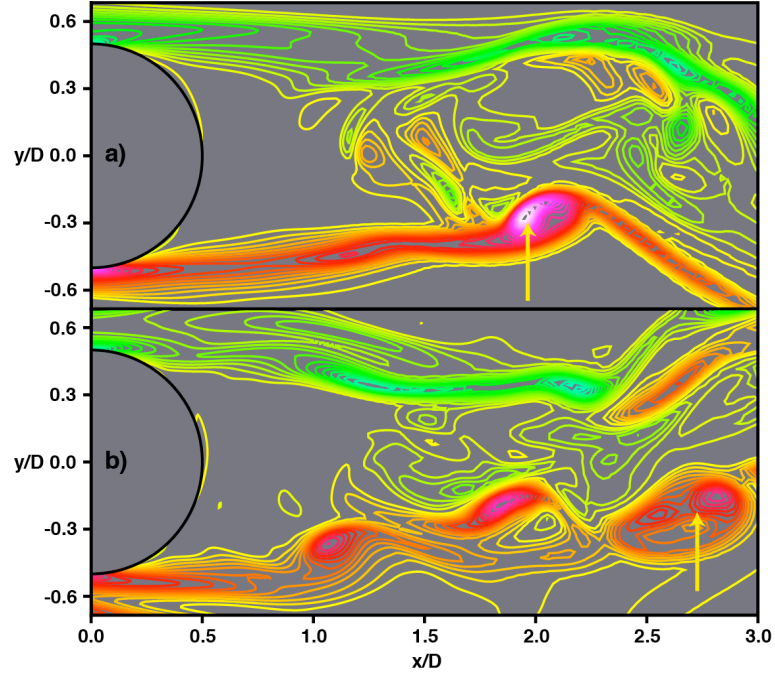
Fig. 9. Instantaneous contours of spanwise vorticity in an (x, y) plane, Case E (ψ = 4.89, n = 3000), a) z/D = 0.0, b) z/D = 4.0 (midspan).
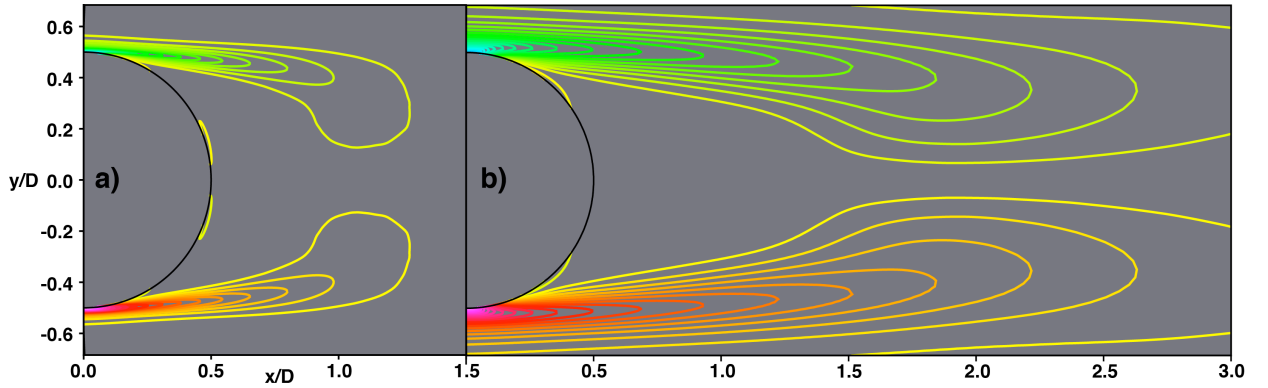

Fig. 10. Contours of time-averaged spanwise vorticity in an (x, y) plane, a) Case A (ψ = 1.00) & b) Case E (ψ = 4.89).

Earlier, in the case of the cylinder, the circulating flow associated with the initial formation of a shed vortex was found to be the result of reverse flow very near and tangential to the base (below the centerline) caused by an earlier shed vortex (positive), the reverse and upward flow (below the centerline) induced by the recently formed negative vortex that moves downward and to the right (going from phase ϕ_A to ϕ_B), and the forward flow in the lower shear layer and further below. It is of interest to determine if the same or a similar process exists in the wake of the flat plate with turbulent separating boundary layers in the case with more conventional shedding, Case A. Because of the highly disturbed nature of the base flow (containing recirculation region vortices, shear layer instabilities etc., see for example Fig. 8a), phase-averaged velocity and pressure fields are used instead of their instantaneous versions. Details regarding the phase-averaging method are provided in Rai (2013). The phase ϕ = 0.0 (0.0 ≤ ϕ ≤ 1.0) corresponds to the phase when the center of the upper shed-vortex is located at x/D = 5.5.

Figure 11 shows phase-averaged velocity vectors and pressure contours at the phase ϕ = 0.24 in Case A. The location of the center of the upper shed vortex is evident. As in Fig. 1a for the cylinder, the

flow below the wake centerline moves downward and then turns sharply to the right. Circulating flow below the wake centerline is absent at this phase.
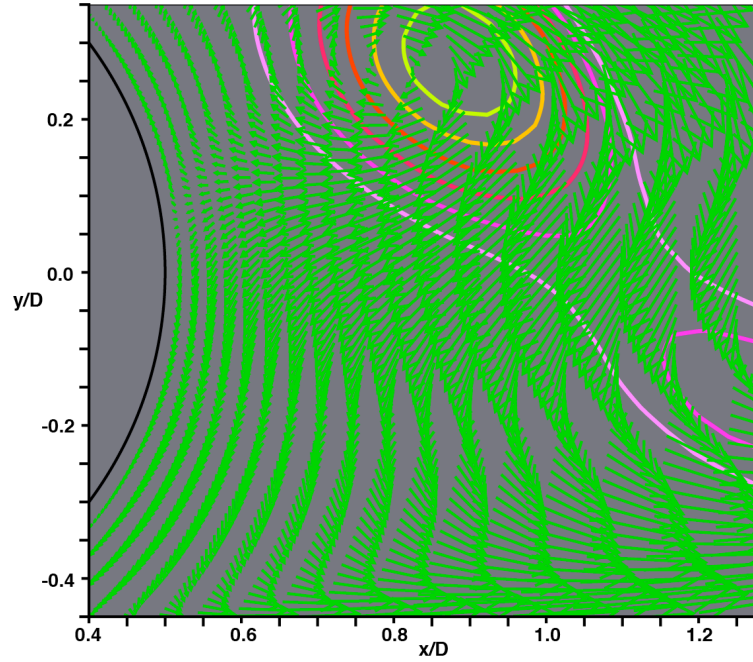

Fig. 11. Phase-averaged velocity vectors and pressure contours, Case A, ϕ = 0.24 (vectors constructed only at 5% of the grid points).
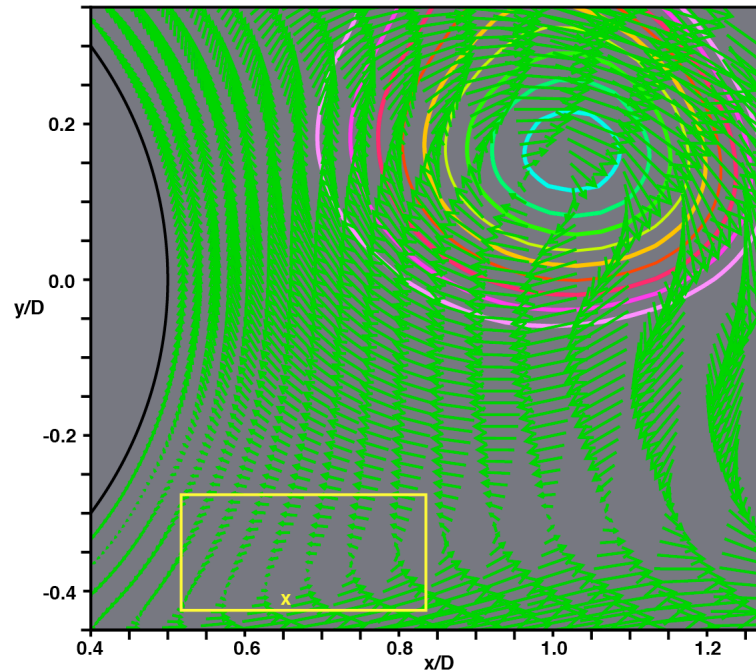

Fig. 12. Phase-averaged velocity vectors and pressure contours, Case A, ϕ = 0.44 (vectors constructed only at 5% of the grid points, point X located at x/D = 0.65, y/D = -0.41).

Figure 12 shows phase-averaged velocity vectors and pressure contours shortly thereafter at ϕ = 0.44. As in Fig. 2a for the cylinder, the upper shed vortex has moved downward and to the right, and

causes flow reversal below the centerline. The flow in the shear layer region is to the right and upward. The flow very near the base continues to be downward (remnant of the flow induced by the previous positive shed vortex). Again we have the essentials for circulating flow. The result is the region of circulating flow within the rectangle. The symbol x marks the location of the pressure minimum. Figures 1 - 3 and Figs. 11 – 12 indicate that the shedding process in Case A, in a phase-averaged sense, is similar to that of the cylinder. This is interesting given the extreme complexity of the wake flow in Case A with turbulent separating boundary layers, the instability of the detached shear layers and presence of recirculation region vortices.
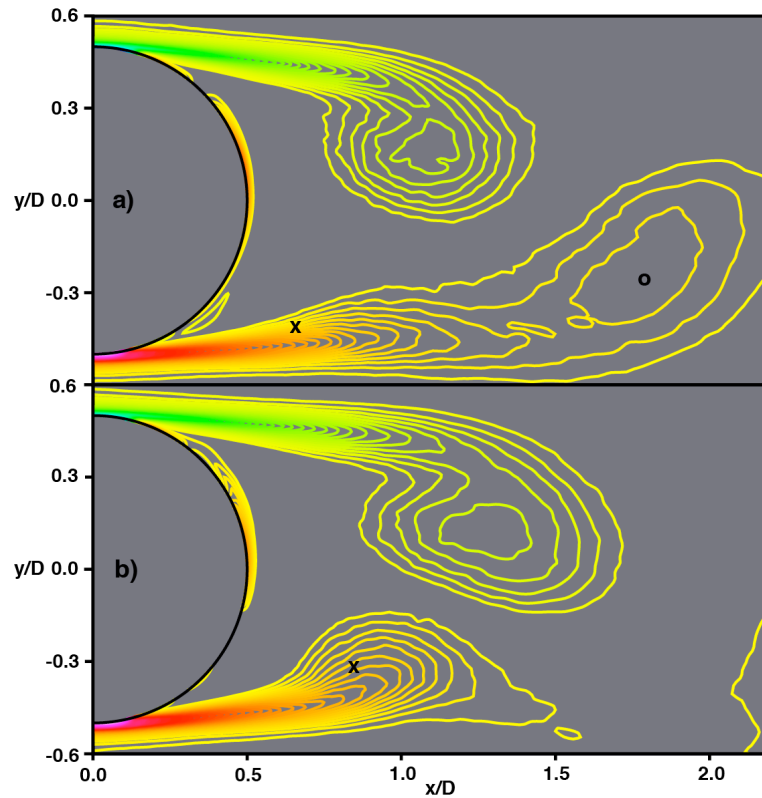

Fig. 13. Phase-averaged spanwise vorticity for Case A at a) $\phi = 0.44$ and b) $\phi = 0.68$.

Figure 13 shows phase-averaged spanwise vorticity contours at vortex initiation, $\phi = 0.44$, and at the later phase, $\phi = 0.68$. The pressure minimum initially occurs near the inner edge of the lower shear layer (marked with an x in Fig. 13a). Shear layer roll-up is minimal at this phase. In Fig. 13b, circulatory flow induced by the two shed vortices causes a redistribution of the shear layer vorticity that results in the bulbous appearance of the lower shear layer. A peak in vorticity is not yet apparent. The pressure minimum (again marked with an "x") has moved to the right and toward the centerline. The more mature positive vortex in Fig. 13a (which can be considered the evolved version of the newly formed vortex but at the phase $\phi = 1.44$) exhibits the expected peak in vorticity. The pressure peak associated with this vortex (marked with an "o") is almost coincident with the peak in vorticity.

Vortex shedding in Case F

The reductions in Re_D in cases D and E in comparison to Case A resulted in the initiation of deterioration in the shedding process. The focus now is on Case F where Re_D is a quarter of that of Case E while Re_θ is approximately the same (this results in ψ being 20.43 in Case F). As mentioned earlier the spanwise extent of the computational domain in Case F (not normalized by D) is the same as in Case D.

However, in terms of the diameter, it is 32.0D (Case F). Some of the observed shedding characteristics obtained in Case F, which are significantly different from the earlier cases, are discussed below.

A top view of instantaneous surfaces of constant negative λ_2 (λ_2 being the second eigenvalue of $\boldsymbol{S}^2 + \boldsymbol{\Omega}^2$, see Jeong & Hussain, 1985) in the region -1.0 < y/D < 1.0, for Case F are provided in Fig. 14.
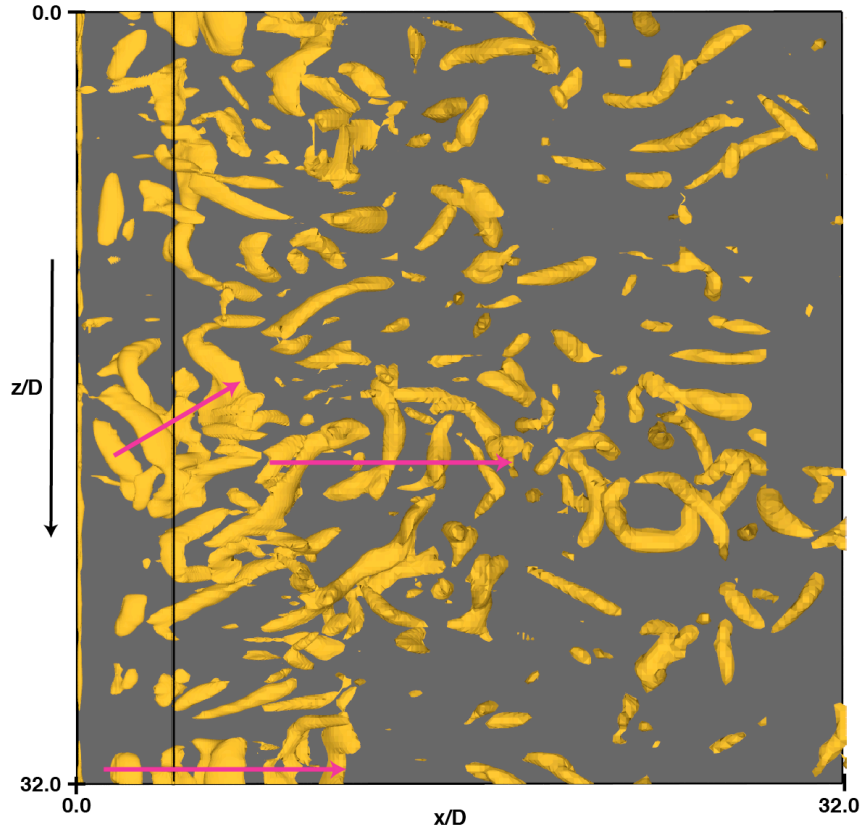

Fig. 14. Instantaneous surfaces of constant λ_2 (negative) in the region -1.0 < y/D < 1.0, Case F, (top view, ψ = 20.43, n = 200,000).

While surfaces of constant pressure also show similar features, surfaces of constant negative λ_2 more clearly depict the vortices in this particular case. The vorticity field in Case F is considerably different than that obtained in Cases A, D & E (Figs. 6a, 6b & 6c). Sequences of approximately spanwise vortices, between 1.0D & 4.0D in length, are evident. Some of the sequences are marked with arrows. While two of the marked sequences show vortices well aligned with the z direction, one of them occurs at an angle of approximately 30°. Some of the vortices are even aligned with the x direction and are probably streamwise vortices from the upstream boundary layers.

The two most significant features of Fig. 14 are a) the spanwise vortices are of finite length in the z direction and b) the sequences are also finite. If indeed the sequences comprise shed vortices, then *shedding seems to be intermittent in Case F*. Some of the questions that Fig. 14 raises are as follows: Are the spanwise vortices shed vortices? If so, is the shedding process similar to the more conventional shedding of Cases A & D? What is the cause of the observed intermittency in shedding? What causes the shed vortices to be of finite length? How does the spectrum obtained for the cross-stream velocity in Case F compare with that of Case D at the wake center-plane? Does the spectrum have a sharp peak? How do the fluctuations in velocity compare in the two cases? Some of the answers are provided here.

Figure 15 shows contours of instantaneous spanwise vorticity at z/D = 0.0 and at the same time instant as in Fig. 14. Firstly, the upper and lower detached shear layers have nearly merged very close to the trailing edge, hence the separation distance between the two, that was discussed with regard to the earlier cases, is essentially non-existent. There is very little room for a traditional shear-layer roll-up, given the thickness of the detached shear layers in relation to the diameter of the trailing edge. Instead, the shed vortices (positive ones marked with blue arrows and negative ones with red arrows) are essentially confined to the shear layers for about the first fifteen diameters (it will become evident shortly that these are indeed shed vortices). Beyond 20 diameters the shear layers breakdown but the vortices persist. The vortices seen in the first 12 diameters are also seen in Fig. 14 (the sequence closest to the lower and upper boundaries in Fig. 14). Although a conventional roll-up is largely prevented by the proximity of the shear layers, the shed vortices, because of their combined induced velocity field, result in shear layers that are sinuous in appearance. Also evident in Fig. 15 are the log-layer eddies from the upstream boundary layers, further removed from the centerline, convecting downstream. Clearly, some of the observed shedding characteristics in Case F are significantly different than in Cases A & D.
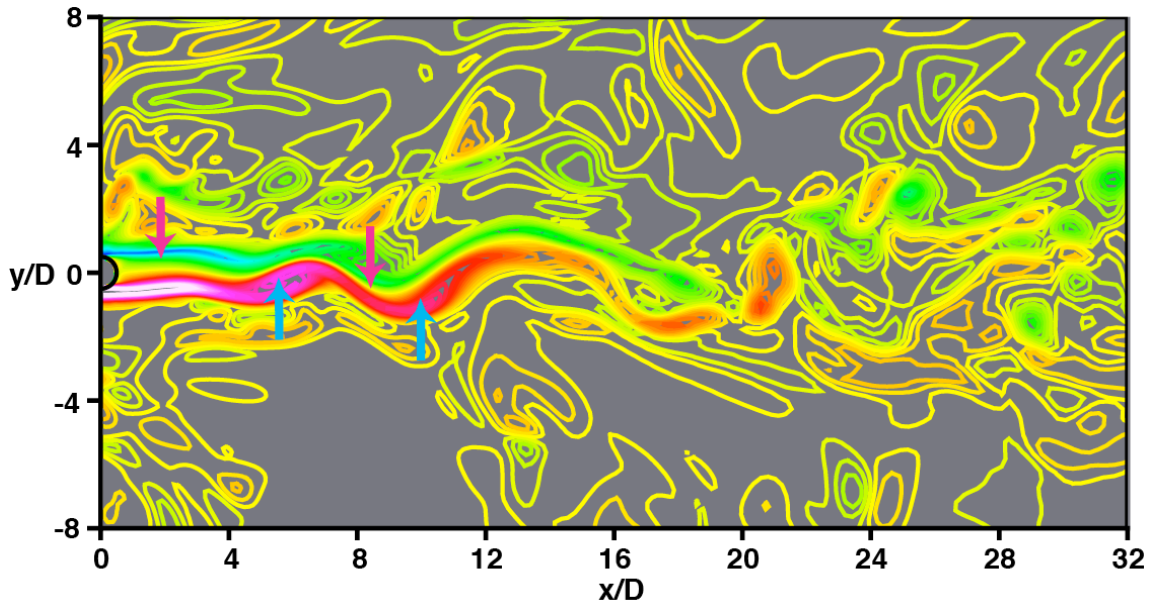

Fig. 15. Instantaneous contours of spanwise vorticity in a (x, y) plane, Case F (ψ = 20.43, z/D = 0.0, n = 200,000).

Shed vortices close to the wake center-plane result in cross-stream flow at this plane, with downwash between a negative/positive shed vortex pair (vortices occurring in that order in the streamwise direction) and upwash between a positive/negative vortex pair. Figure 16 shows contours of cross-stream velocity v over 20 shedding cycles in the (t, z) plane for Case D at x/D = 4.0, y/D = 0.0 (the location x/D = 4.0 was chosen because the shed vortices in Case D are well formed at this location). Here and in the following figures T_p is the shedding period. The figure shows bands that are nearly vertical.
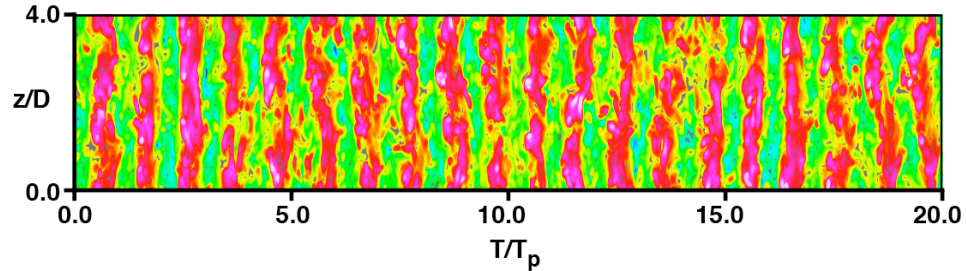

Fig. 16. Contours of cross-stream velocity at x/D = 4.0, y/D = 0.0 (Case D, ψ = 2.28).

As expected, the bands are similar to the ones seen in Fig. 7b around x/D = 4.0 (which shows contours of instantaneous *v* in the wake in the *(x, z)* plane for Case D).

Figure 17 shows *v* over 20 shedding cycles in the (t, z) plane for Case F at x/D = 1.0, y/D = 0.0. Only half of the spanwise extent of the computational domain is included in this figure, and contours corresponding to values of *v* close to zero have been omitted for clarity. For reasons that will be obvious shortly, the x location chosen for Case F is closer to the base than in Case D (Fig. 16). However, the patterns obtained at x/D = 4.0 are quite similar to those obtained at x/D = 1.0, except that they occur later in time. The features discussed earlier with regard to Fig. 14 are also evident here. The bands on average are between one and four diameters in length. They occur in sequences whose lifetimes vary and consist of pairs of opposing color (upwash/downwash). The differences between Figs. 16 & 17 are striking.
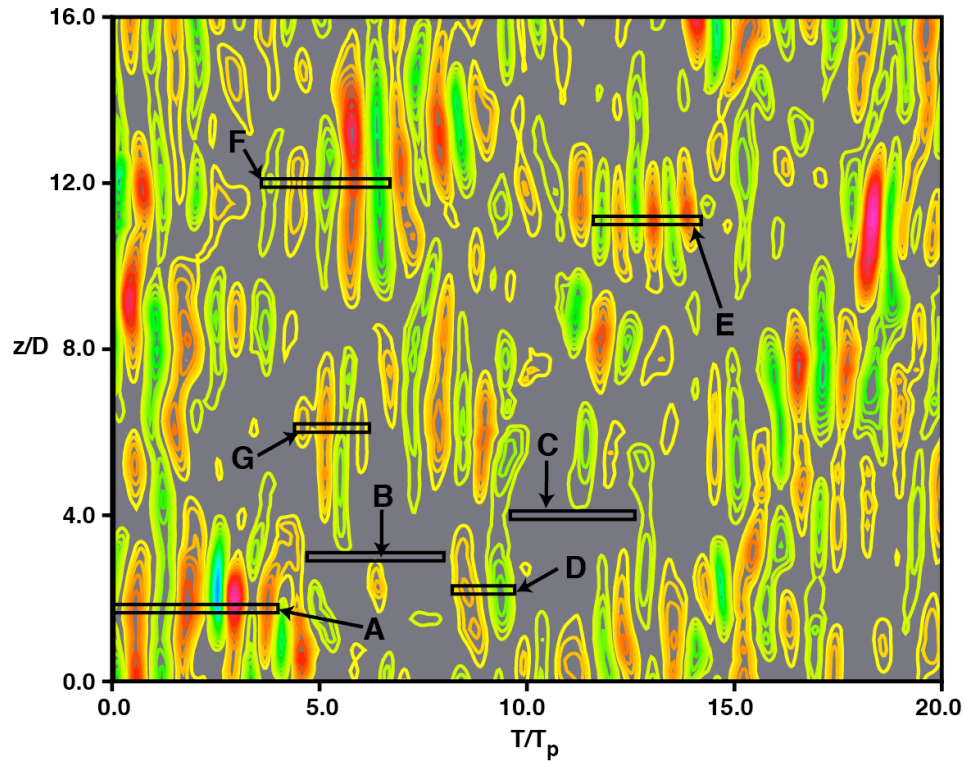

Fig. 17. Contours of cross-stream velocity at x/D = 1.0, y/D = 0.0 over 20 shedding periods (Case F, ψ = 20.43).

The bands in Fig. 17 show the relation between the shed vortices of Fig. 14 and upwash/downwash in the wake center-plane. The spaces between the sequences of bands (inter-sequence spaces) are of importance. The spaces that occur between sequences (in the T direction) may provide insight into *possible* intermittency. For example, why do sequences weaken and taper off? Similarly, spaces between sequences in the z direction may shed light on the reasons underlying the finite length of the bands (and associated shed vortices). Potential inter-sequence spaces for further study were selected by first plotting a large number of contours but with the same minimum/maximum values of *v* as in Fig. 17 and then picking those regions with very few or no contours. It was determined via (x, y) plots of instantaneous spanwise vorticity, in the regions thus selected, that occasionally shed vortices of nominal strength were present but the detached shear-layer in which they were embedded was displaced significantly from the wake center-plane because of large fluctuations in the separating boundary layer. The displacements are sufficiently large to cause a significant weakening of upwash/downwash at the center-plane. The shed vortices during these periods can be visualized by choosing a larger range of y in Fig. 14. However, at other times the detached shear layers become relatively quiescent and the instability

manifests very weakly. It is possible that the disturbances present in the separating boundary layer interfere with the shed-vortex formation process. The nature of this interference is yet to be determined.

An exploration of the shedding process and its continuity/intermittency in time

It is of considerable importance to determine if shedding is continuous or intermittent in time. Both contours of v and surfaces of constant λ_2 indicate possible intermittency in time. Here we use another attribute associated with vortex shedding to explore the phenomenon in greater depth. Figure 18a shows contours of instantaneous spanwise vorticity for the cylinder case discussed earlier.
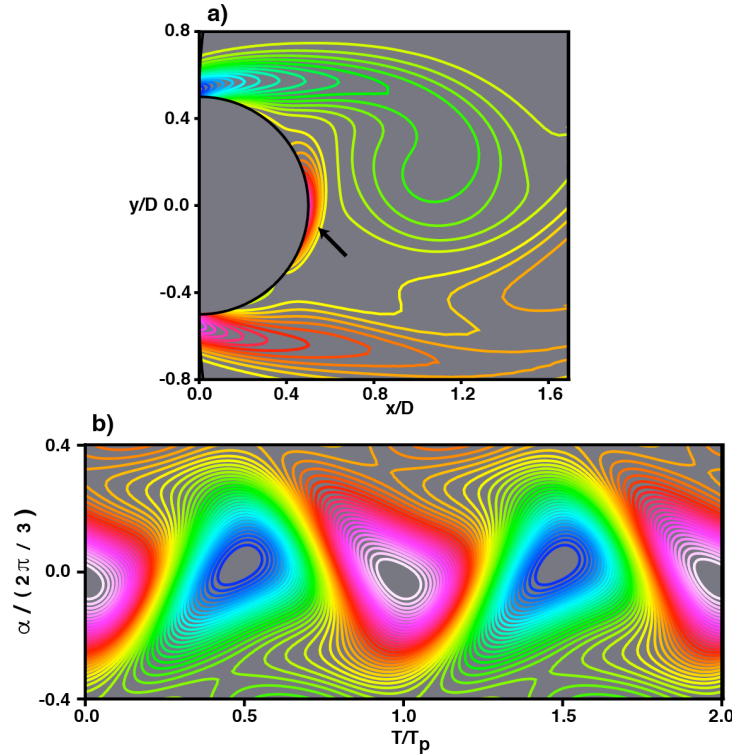

Fig. 18. a) Contours of instantaneous spanwise vorticity for the cylinder and b) time variation of spanwise vorticity on the downstream surface of the cylinder over two shedding periods.

The figure shows a well-formed upper shed vortex (negative spanwise vorticity). The resulting recirculating flow in the base region causes the near-surface spanwise vorticity to be of the opposite sign (see arrow). The development of the next shed vortex (positive) results in the near surface spanwise vorticity becoming negative. Figure 18b shows the time variation of the spanwise vorticity on and along the rear surface of the cylinder (angular distance α varies from -60° to +60°), over two shedding periods. The periodic variation of near-surface vorticity is evident. This method of sensing vortex shedding detects weak shed vortices (as will be seen shortly). The extent of the base that experiences noticeable fluctuating spanwise vorticity depends on the strength/size and position of the shed vortices; vortices confined to one side of the wake center-plane tend to affect only the corresponding half of the base.

Regions A & B in Fig. 17 span periods in time, and z locations at which shedding-related upwash/downwash and little to none at all, exist, respectively. Figure 19a shows the time variation of surface spanwise vorticity on the circular trailing edge of the flat plate (-60° ≤ α ≤ 60°) associated with Region A (four shedding periods). The elevated regions of vorticity associated the positive/negative vortices are evident; significant variation in shedding periods and shed-vortex strength are also observed. Figure 19b shows corresponding contours for Region B (over 3.3 shedding periods).
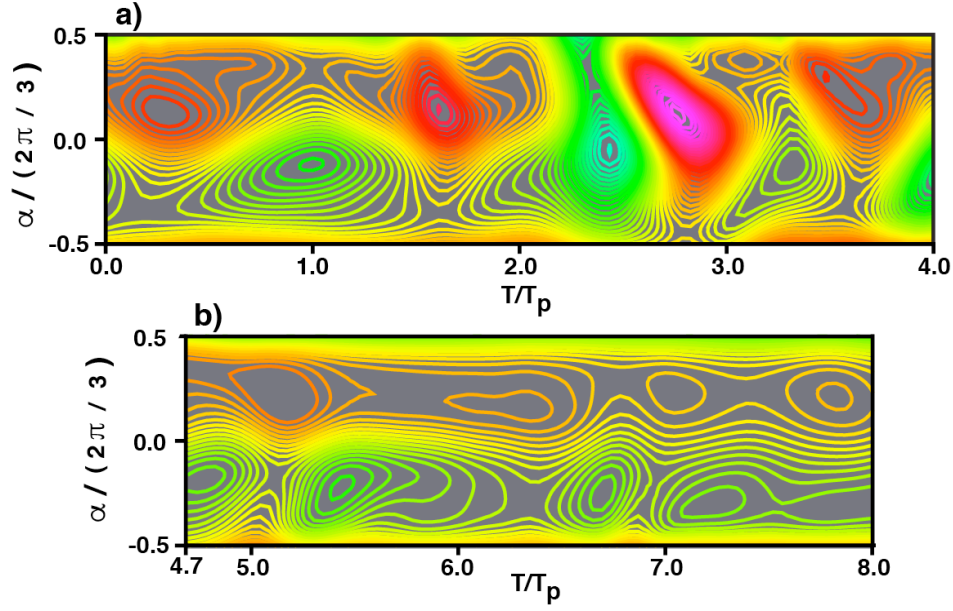
Fig. 19. Contours of surface spanwise vorticity as a function of time and α for case F ($\psi = 20.43$), a) Region A & b) Region B.

The minimum/maximum vorticity levels and the number of contours specified to obtain Figs. 19a & 19b are the same; these two subplots can be directly compared. Figure 19b clearly indicates vortex shedding in Region B albeit very weak shedding. Shedding (circulating flow) was confirmed by animations of velocity vector plots as well. The shed vortices at formation, both in Regions A & B, are largely confined to either the upper or lower half of the base region. This results in the positive/negative regions of surface spanwise vorticity also being largely confined to the upper/lower halves of the base region, respectively.
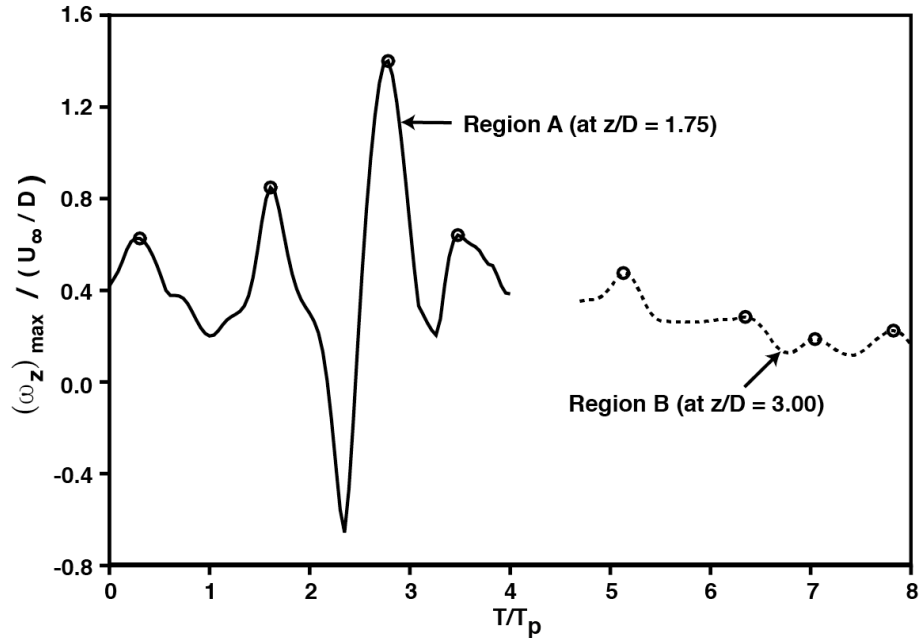

Fig. 20. Highest (positive) value of surface spanwise vorticity as a function of time for Regions A & B.

In an effort to quantify shedding strength obtained in Regions A & B, the highest value of surface spanwise vorticity ($-60° \leq \alpha \leq 60°$) at the each instant was obtained (normalized with plate thickness and freestream velocity). Figure 20 shows the time variation of this vorticity value (the value is negative at

times). The maxima in the curves are associated with the occurrence of negative shed vortices in Regions A & B (the circles depict maxima in time). As expected the fluctuations obtained for Region B are considerably weaker than those obtained in Region A. *However, the point of significance here is that, although the shedding process is greatly weakened during certain periods of time, it is continuous.* Region C in Fig. 17 (quiescent region) also exhibits surface vorticity characteristics similar to that of Region B.

The shed vortices in Case F form between x = 0.8D & 1.2D (center of circulating flow). Their effect if any, is felt almost immediately in the vicinity of the location x/D = 1.0 on the wake center-plane. This results in a direct correlation between the regions depicted in Fig. 17 (obtained at x/D = 1.0) and increasing/decreasing surface spanwise vorticity. In contrast, a choice of say x/D = 4.0 in Fig. 17, would require a lag to be introduced in Fig. 19 to take into account vortex travel time to x/D = 4.0.

Earlier, in Figs 11 & 12, the shedding process in Case A was investigated with the aid of phase-averaged velocity vectors and pressure contours.
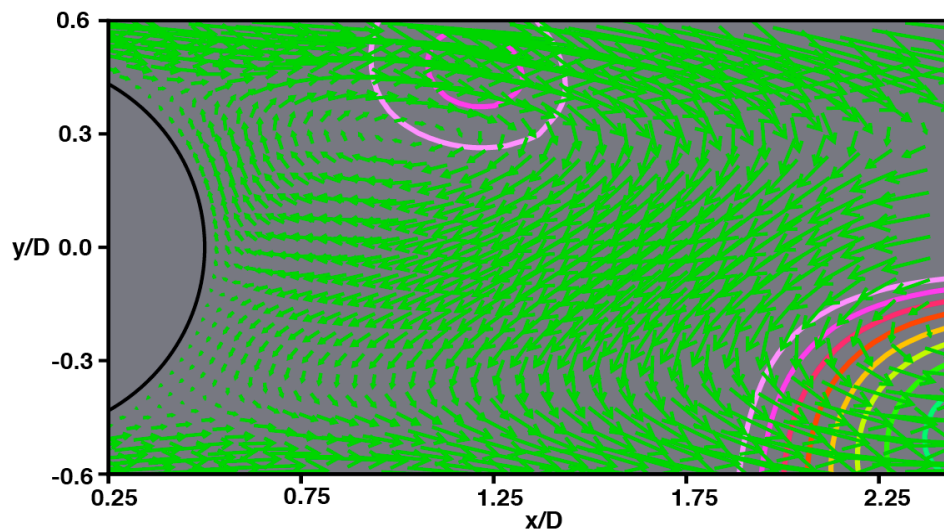

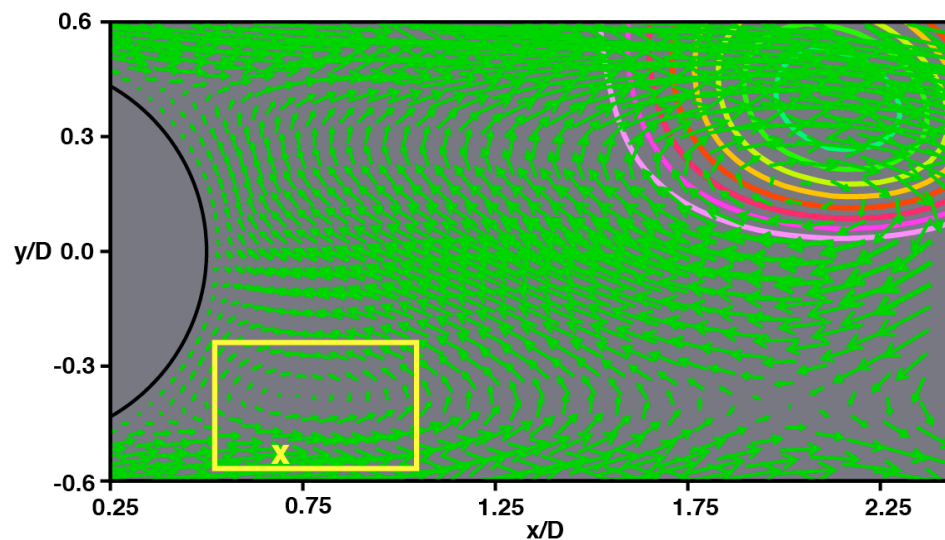Fig. 21. Instantaneous velocity vectors and pressure contours, Case F (ψ = 20.43, z/D = 0.0, n = 180,280).

Fig. 22. Instantaneous velocity vectors and pressure contours, Case F (ψ = 20.43, z/D = 0.0, n = 180,440).

The process was found to be quite similar to that encountered in the case of the cylinder. Here again, in Case F, with all its complexity, one would like to ascertain if there are differences in the *initial* causes for circulating flow. Figures 21 and 22 show velocity vectors and pressure contours at two instants in time (separated by a fraction of the shedding period). These figures are counterparts of Figs. 11 & 12, respectively, except for the fact that instantaneous flow variables are used instead of phase-averaged variables (the more quiescent base region, absent recirculation region vortices etc. makes this possible). As in the case of the cylinder and the thick flat plate (Case A), the essential components for circulatory flow appear with the downstream movement of the upper shed vortex. The result is the circulating flow within the rectangular region. This process was observed repeatedly. Clearly, the initiation of shedding in Case F is similar to that of the cylinder.

Variation in shedding period

The contours of cross-stream velocity in Fig. 17 show that the shedding period (width of pairs of vertical bands) varies from event to event (sometimes even within an event). In some instances the ratio of shedding periods between events is significant. For example, this ratio between Regions D & E is approximately 1.6. The most probable cause is the turbulent nature of the separating boundary layer. Fluctuations in the streamwise velocity within the boundary layer could potentially slow down or hasten the convective rate of the shed vortices that are confined to the detached shear layer (as in Fig. 15) and thus increase/decrease the shedding period. To explore this theory, the near-surface fluctuating component of the streamwise velocity (u') within the boundary layer was examined at and upstream of $x/D = 0.0$, and at $(y - y_{wall})/D = 0.0658$ (and various appropriate z locations of choice).
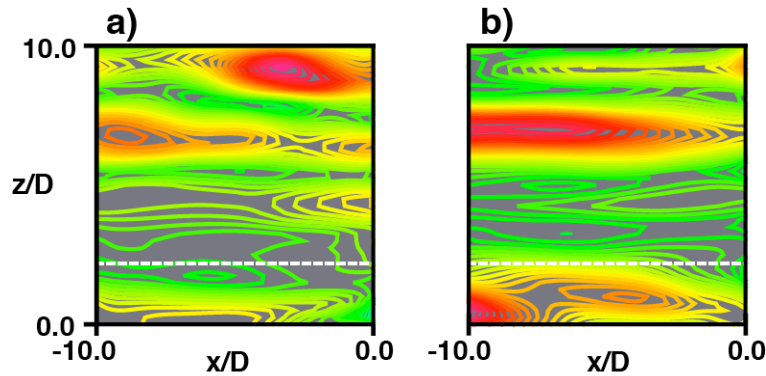

Fig. 23. Contours of instantaneous u' above the plate surface, a) at the beginning and b) at the end of the event in Region D.
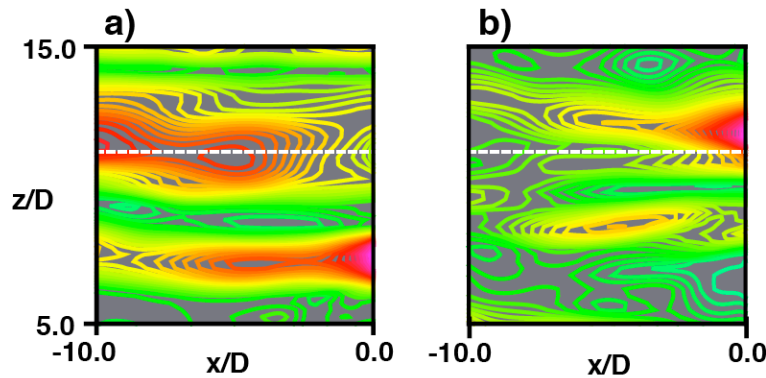

Fig. 24. Contours of instantaneous u' above the plate surface, a) at the beginning and b) at the end of the event in Region E.

Figures 23a and 23b show contours of instantaneous u′ at the beginning and end of the time period corresponding to Region D in a (x, z) plane above the plate surface. The dashed white line at z/D = 2.2 corresponds to the center of the rectangle containing Region D in Fig. 17. High and low speed regions are evident in both these figures. Clearly, there is a low speed region at x/D = 0.0 both at the beginning and end of the time period corresponding to Region D. This is in accordance with the theory proposed earlier (lower streamwise velocities result in larger shedding periods). Figures 24a and 24b show contours of u′ as in Figs. 23a & 23b but at the beginning and end of Region E. The dashed white line corresponds to the center of Region E. The large high-speed region approaching the point x/D = 0.0 in Fig. 24a is evident. It travels over the point x/D = 0.0 during the time period corresponding to Region E. This again is in accordance with the proposed causative agent (higher streamwise velocities reduce the shedding period).

Figure 25 shows the time variation of u′ at x/D = 0.0 during the periods corresponding to Regions D & E (at the appropriate z locations). The figure also shows the time-average of u′ (over the same time periods). In region D, the value of u′ is negative during the entire event (accordingly the average is negative as well). In Region E, the value of u′ is essentially positive (except at the beginning). The average value during the event is positive. The results of Figs. 23 – 25 clearly indicate that high and low speed streaks decrease and increase shedding period, respectively.
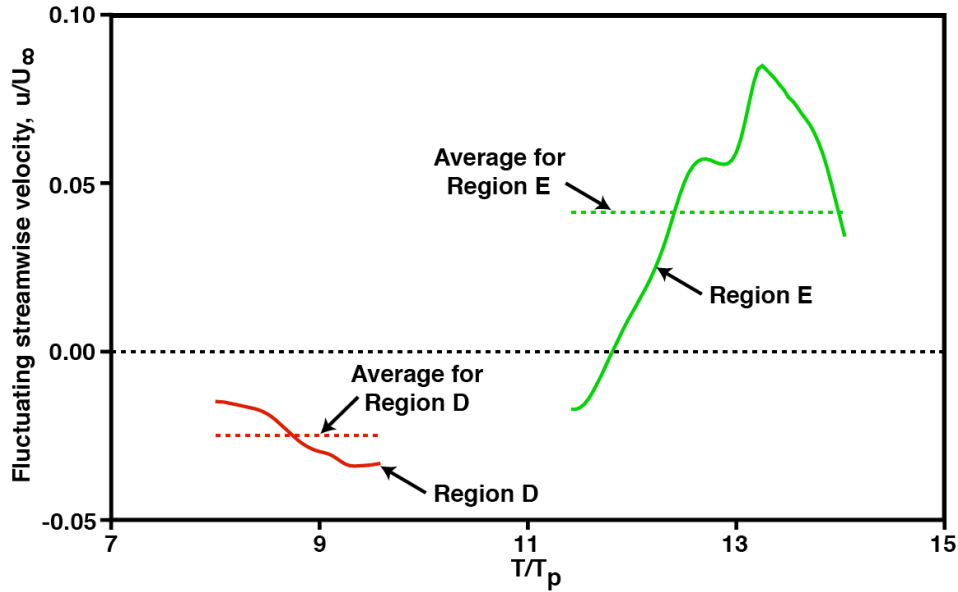

Fig. 25. Time variation u′ (and corresponding average) at x/D = 0.0 during shedding Regions D & E.

Regions F & G (high & low shedding periods, respectively) were also investigated in a similar manner. The time-averaged values of u′ (during the events) in these two cases are -0.0382 & 0.0613 (normalized by the freestream velocity), respectively. The corresponding values for the cases D and E are -0.0249 & 0.0414, respectively. Unlike in Case E, u′ did not change sign during events F and G. Thus, cases F & G provide further evidence that high-speed streaks decrease the shedding period and low-speed streaks have the opposite effect. *Thus boundary layer fluctuations in streamwise velocity can significantly alter the shedding period.*

Time-lags corresponding to the approximate time required for the flow features in the boundary layer to convect from X/D = 0.0 to x/D = 1.0 (where the shed vortices first appear) have been accounted for in obtaining Figs. 23 - 25. These time lags were obtained by tracking easily observed features in animations of u′ in a (x, z) plane above the plate surface (as in Figs. 23 & 24).

The variations in shedding period in Case F can be expected to widen the peak associated with shedding in spectra of fluctuating cross-stream velocity. Figure 26 shows spectra for fluctuating v at x/D = 4.0 on the wake center-plane for Cases D & F. Both of them show a peak at shedding frequency ω_{st}. However, Case D exhibits a sharp peak whereas in Case F, as expected, the peak is wide. In the investigation of the instability of the detached shear layer of the cylinder, Rai (2010), it was found that the time-variation of the shear-layer vortex generation rate was much less than indicated by the energy spread in the spectrum of the fluctuating velocity signal (obtained near the shear layer). The analysis showed that amplitude modulation (generally increasing amplitude during the first half of a period of instability followed by decreasing amplitude during the second half), could be a significant contributor to the broadening of the peak associated with the shear-layer instability. Figure 17 shows amplitude modulation in the shedding events of Case F. Thus, the broadening of the spectrum seen in Fig. 26 may not be entirely because of variation in shedding frequency but also partly due to amplitude modulation.
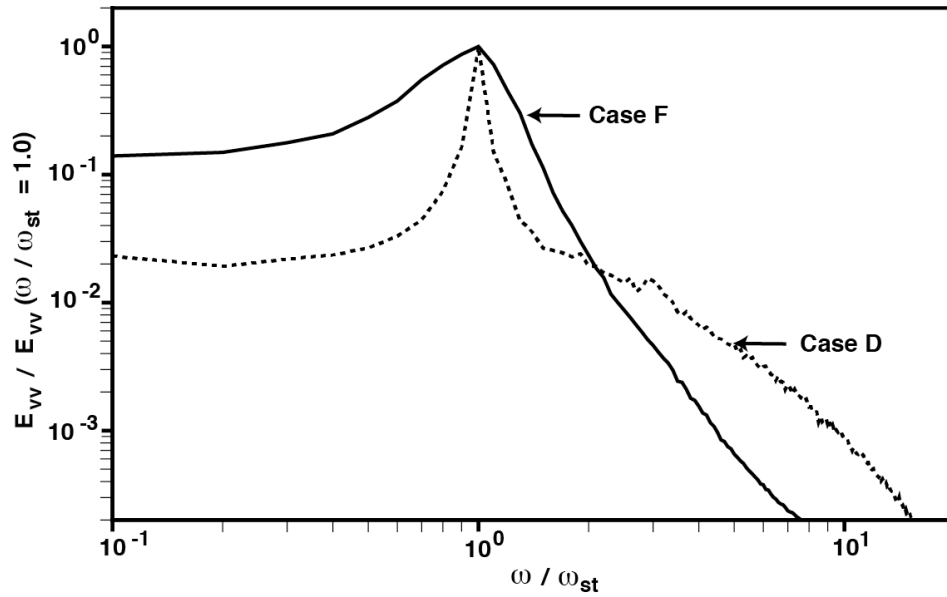

Fig. 26. Comparison of spectra obtained for fluctuating v in Cases D & F, (ψ = 2.28 & 20.43, x/D = 4.0).

Time-Averaged Velocity Statistics in the Wake for Cases D & F

The distribution of time-averaged velocity statistics (also averaged in the z direction) in the wake region for Cases D and F are presented in this section. Earlier investigations by Rai (2013 & 2014) have included phase-averaged velocity statistics; this is difficult (for reasons discussed earlier) and also of limited utility in Case F. Distributions of time-averaged values of velocity components and spanwise vorticity are presented first followed by distributions of time-averaged fluctuating kinetic energy and shear stress. Fluctuations include those due to quasi-periodic shedding and the random component. *The specified minimum and maximum values and the numbers of contours in the subplots in the following figures are identical; the subplots within a given figure may be directly compared.*

Figures 27a and 27b provide contours of time-averaged streamwise velocity u for Cases F & D, respectively. The dashed white line corresponds to u = 0.0; thus the region between the base and this line consists of reverse flow. The separated region obtained in Case F is significantly larger in size although separation occurs sooner on the trailing edge surface in Case D. The zero contour line crosses the wake centerline at 1.87D and 3.12D for cases D and F, respectively. Peak reverse flow occurs at 1.41D and 1.77D for cases D and F, and the ratio of peak negative u values in the two cases is 2.73 (D to F). As expected, reverse flow in Case F is much weaker. The color palette indicates a more rapid recovery of u past the u = 0.0 contour line both in the x and y directions in Case D.
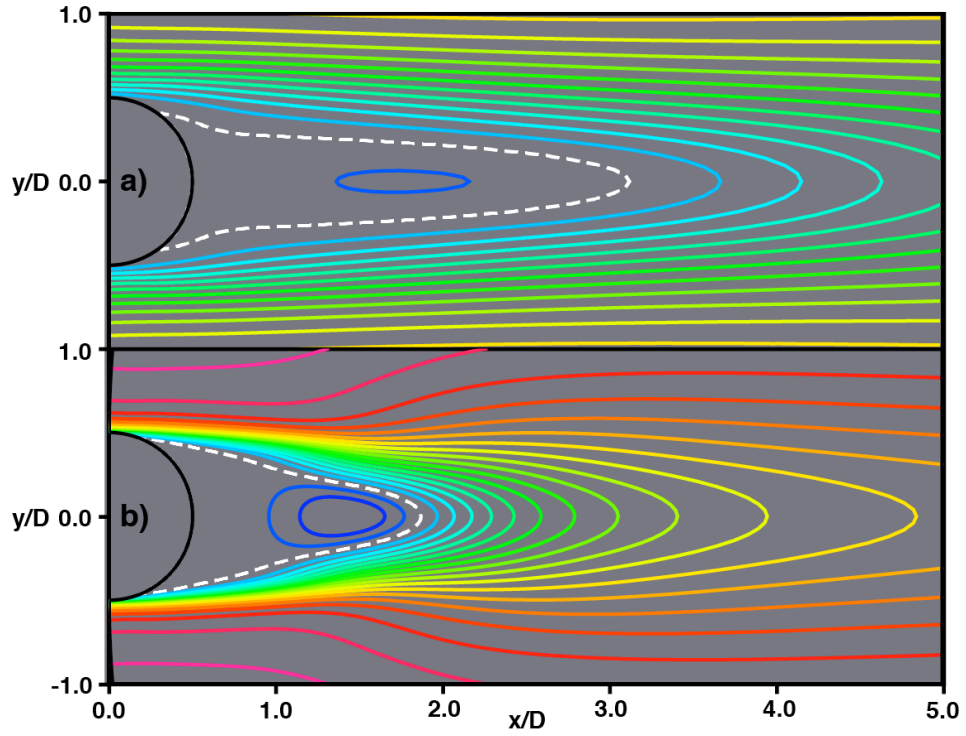
Fig. 27. Contours of time-averaged u, a) Case F ($\psi = 20.43$), b) Case D ($\psi = 2.28$).

Contours of time-averaged cross-stream velocity v for Cases F and D are shown in Figs. 28a and 28b, respectively. A positive peak at $x/D = 1.07$ and a negative one at $x/D = 1.74$ in the upper half of the plane are evident in Fig. 28b.
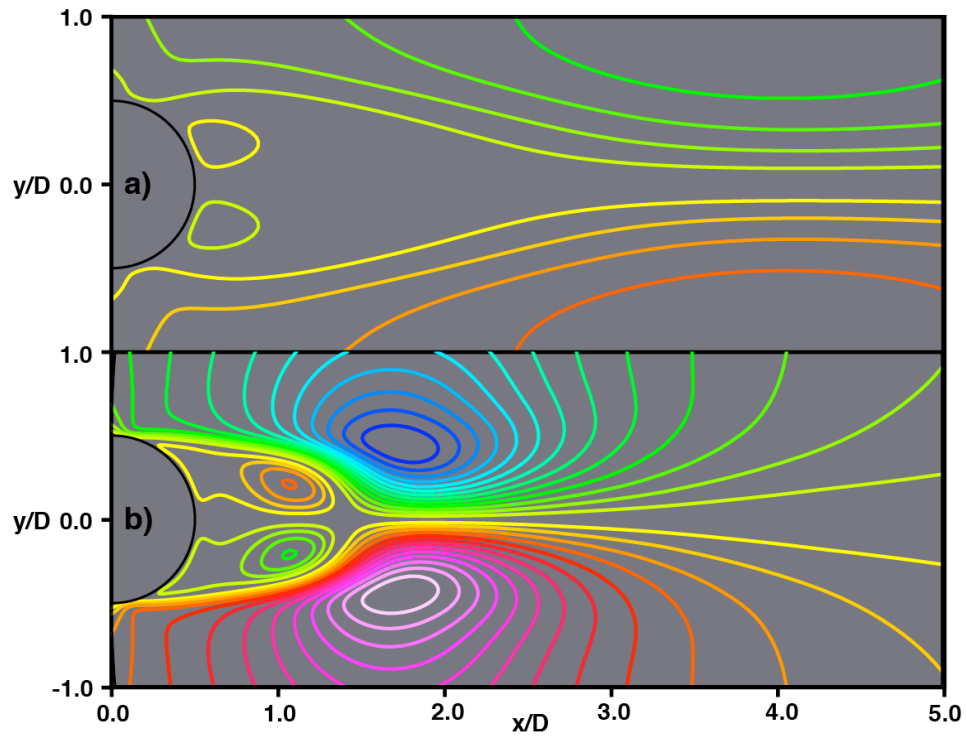

Fig. 28. Contours of time-averaged v, a) Case F ($\psi = 20.43$), b) Case D ($\psi = 2.28$).

These two peaks indicate the reverse flow in the base region and the induced cross-stream flow caused by the negative shed vortices, respectively. The contours obtained in the lower half are a reflection of those seen in the upper half (with a sign change). The data in Case F (Fig. 28a) are qualitatively similar but the cross-stream flow is considerably weaker. The positive peak in the upper half of the plane occurs close to the base and is associated with the reverse flow in this region. The negative peak, however, is relatively quite distant from the base; it occurs at x = 3.74D. Centerline cross-stream intensity level at a given streamwise location and average shed-vortex strength at the same location are directly related (through the upwash/downwash at the centerline resulting from the passage of the shed vortices). As will be seen shortly, the centerline cross-stream intensity level peaks at x = 8.14D in Case F (although there is little variance of this quantity between 6D and 10D). In Case D the peak occurs at 2.09D. Thus, peak shed-vortex strength occurs much further downstream in Case F compared to Case D. Correspondingly, the peak in negative v (in the upper half of the plane) also occurs at a larger value of x/D.

Figures 29a and 29b show contours of time-averaged spanwise vorticity for Cases F and D, respectively. Contours corresponding to vorticity values close to zero have been omitted in Fig. 29. The detached shear layers (DSLs) and the corresponding regions of higher vorticity are seen located substantially away from the centerline and only for x/D < 2.0 in Case D.
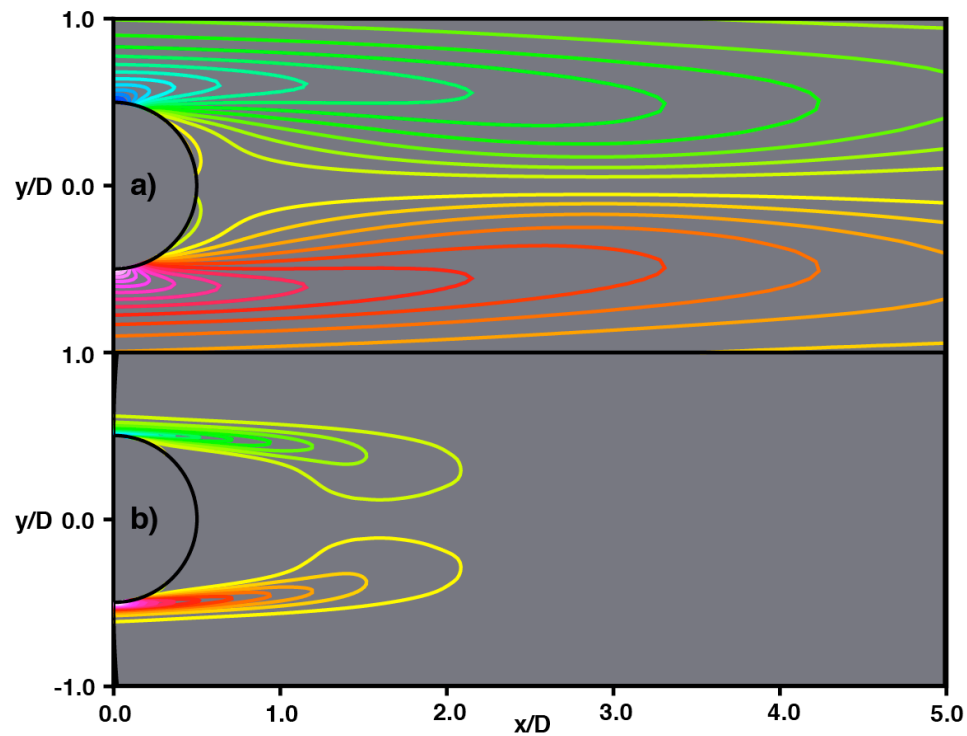

Fig. 29. Contours of time-averaged spanwise vorticity, a) Case F (ψ = 20.43), b) Case D (ψ = 2.28).

In Case F the DSLs extend beyond x/D = 5.0. In addition there is little separation between the two DSLs from about x/D = 1.0 onwards in Case F, thus indicating the strong interaction between them and the difficulty in a shear-layer roll-up that accompanies the conventional shed-vortex formation process.

Figure 30 shows the variation of streamwise and cross-stream normal intensities with x/D along the centerline for Cases D & F. While peak values of streamwise intensity are roughly the same (Case D shows a slightly larger peak), peak cross-stream intensity levels are substantially different. The peak value in Case D is larger by a factor 6.64 and occurs closer to the base. The reason for this has been discussed earlier (weaker shed vortices in Case F that reach their peak strength further downstream). A

second difference between the two cases is that while the peak in cross-stream intensity is higher than the peak in streamwise intensity in Case D, the reverse is true in Case F. The primary cause for the reversal in trend is again the relative weakness of the shed vortices in Case F that results in significantly diminished cross-steam intensity levels. While the streamwise intensity level is also somewhat diminished in Case F, much of it is inherited from the boundary layer and therefore is not affected to the same extent.
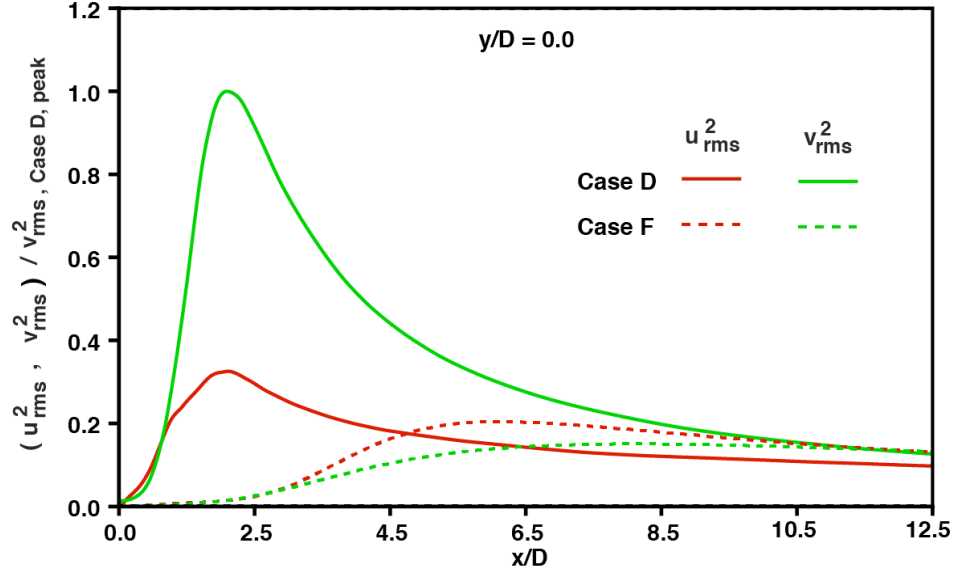

Fig. 30. Variation of streamwise and cross-stream intensities along the wake centerline for Cases D & F.

Figures 31a and 31b show contours of time-averaged fluctuating kinetic energy (all three-components, including both random and quasi-periodic fluctuations).
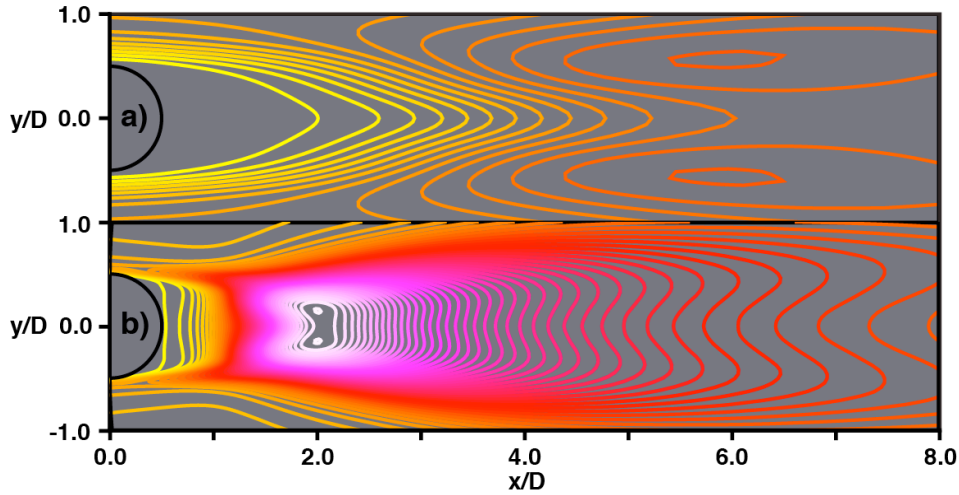

Fig. 31. Contours of time-averaged fluctuating kinetic energy, a) Case F ($\psi = 20.43$), b) Case D ($\psi = 2.28$).

While they are topologically similar, feature scales and locations are substantially different, again, because the region in which shed vortices are strongest is further downstream in Case F when compared to Case D. As expected both figures show non-zero levels in the turbulent separating boundary layers. A peak in intensity is observed in both cases. However, the peak in Case D is higher (stronger shed

vortices) and occurs closer to the base (3.69 times higher and located at x/D = 2.00 instead of 5.93 as in Case F). In addition, peak values in Case D, unlike Case F, occur very close to the centerline. This is because shed vortices in Case D are still in the final stage of formation at x/D = 2.0 and are close to the centerline.

Contours of time-averaged fluctuating shear stress for Cases F and D are provided in Figs. 32a and 32b, respectively. The primary peak values (negative above, positive below) are seen in both cases. The locations roughly correspond to the locations of the peaks in Figs. 31a and 31b. The peak levels obtained in Case D are higher. The reasons for these two attributes are the same as those provided for Figs. 31a and 31b. In addition to the primary peak in Fig. 32b, there exist much weaker secondary peaks (opposite in sign to primary peaks) close to the base (see arrows).
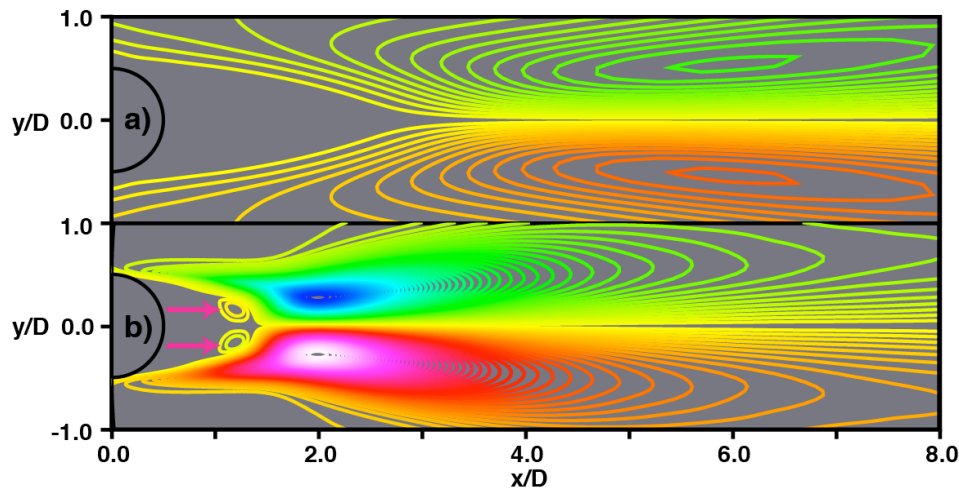

Fig. 32. Contours of time-averaged fluctuating shear stress, a) Case F (ψ = 20.43), b) Case D (ψ = 2.28).

The secondary peaks are present even for Case F but are much too weak to be seen even with the large number of contours used in Figs. 32a and 32b. The origin of the secondary peaks is discussed at length in Rai (2011). It is shown there, in the context of Case A, that they are caused by the *periodic component* of fluctuating velocities resulting from the formation of the shed vortices. The two velocity components are found to be positively/negatively correlated in the vicinity of the upper/lower secondary peak.

CONCLUDING REMARKS

The very near and near wake of a flat plate with a circular trailing edge is investigated with data from direct numerical simulations. Computations were performed for four different Reynolds numbers based on plate thickness (D). The separating boundary layers are turbulent in all the cases investigated. The objective of the study is to understand the changes in wake characteristics as the plate thickness is reduced (increasing θ/D). The value of θ/D varies by a factor of 20.43 in the computations.

The direct numerical simulations of the flat plate wakes show that vortex shedding is vigorous in the low θ/D cases (Cases A and D) and that there is a substantial decrease in shedding intensity as θ/D increases (Cases E & F). In addition a lack of coherence in the spanwise structure of the shed vortices is observed with increasing θ/D. An important finding of the present study is that the interaction between the upper and lower shear layers becomes stronger as D is decreased (keeping θ approximately the same). Also, the proximity of the shear layers (relative to θ) in the large θ/D cases, essentially reduces the ability of the shear layer to roll-up and contribute to the strength of the newly formed shed vortices. In fact, in Case F, the shear layers are so close to each other that the roll-up is essentially prevented and the shed vortices form and remain within the shear layer until the shear layer breaks up.

An initial examination of shedding in Case F via contours of v at the wake center-plane ($t - z$) plane) at a given x location and also the method of Jeong & Hussain (1985, λ_2 criterion) indicated that shedding may be intermittent. The shed vortices were about 1.0D to 4.0D long in the z direction (with some of them occurring at a noticeable angle to this direction). Quiescent regions, between regions of shedding activity, both in time and in the z direction are observed. The former are an indication of potential intermittency in the shedding process. However, a closer look at the shedding process, using fluctuations in trailing-edge surface vorticity, shows that vortex shedding is continuous in time although greatly weakened during certain periods. The active/quiescent regions may be an indication that boundary layer disturbances aid/inhibit vortex shedding.

Another important finding of the present study is that fluctuations in u within the plate boundary layer (near the trailing edge) have a significant effect on shedding period in Case F. High-speed streaks decrease the shedding period and low-speed streaks have the opposite effect. Spectra of v at the wake centerline show a peak for both Cases D & F. However, Case F, as expected shows a broader peak. While fluctuations in shedding period contribute to the broadening of the peak in Case F, some of this broadening may also be a result of amplitude modulation (increasing amplitude of shedding in the first half of a shedding event followed by decreasing amplitude in the second half).

To better understand the *initiation* of the shedding process, shedding was first examined in a far simpler case, that is, the flow past a cylinder at a low Reynolds number. It was determined with the aid of velocity vectors at different phases of the shedding process that the initial circulatory flow in this case is caused by the induced velocities of the previous two shed vortices (positive and negative) and the forward flow in the detached shear layer. The pressure minimum associated with the newly formed vortex and shear-layer roll-up appear later. The circulatory flow associated with the newly formed vortex and the previously shed vortex results in a redistribution of the shear-layer spanwise vorticity that results in the roll-up of the shear layer.

Velocity vector and pressure contour plots are also used in the case of the flat plate to understand the initiation of the shedding process in Cases A & F (lowest and highest θ/D cases computed) and compare it to that of the cylinder. The essential attributes of the initiation process in these two flat plate cases are quite similar to that found in the cylinder wake. The induced velocity fields of the previous two shed vortices and the forward flow in the detached shear layer and further away from the centerline result in circulating flow very near the base in Cases A & F as well.

The effect of changing the ratio θ/D on the time-averaged, near-wake velocity statistics is also provided here (Cases D & F). It was found that increasing θ/D resulted in weakened reverse flow that persists for longer distances (in terms of the thickness of the plate). Contours of time-averaged spanwise vorticity showed that increasing θ/D resulted in decreasing the separation between the upper and lower detached shear layers and increasing their streamwise extent. Peak cross-stream intensity along the wake centerline is substantially lowered with increasing θ/D because of weaker shed vortices. The peak streamwise intensity is also lowered but by a much smaller factor because of the turbulent nature of the separated boundary layer (and thus the inherited streamwise intensity). Interestingly, distributions of the components of velocity, fluctuating kinetic energy and shear stress are found to remain topologically quite similar with changing θ/D. However, the scales and locations of the various features such as maxima/minima are considerably different.

REFERENCES

ALBER, I. E. 1980 Turbulent wake of a thin flat plate. *AIAA Journal*, Vol. 18 (9), 1044.

BURESTI, G., FEDELI, R. & FERRARESI, A. 1997 Influence of afterbody rounding on the pressure drag of an axisymmetrical bluff body. *J. Wind Engng Ind. Aerodyn. 69-71, 179.*

CHEVRAY, R. & KOVAZNAY, L. S. G. 1969 Turbulence measurements in the wake of a thin flat plate. *AIAA Journal*, Vol. 7, 1641.

HAYAKAWA, M. & Iida, S. –I. 1992 Behavior of turbulence in the near wake of a flat plate at low Reynolds number. *Physics of Fluids A*, Vol. 4 (10) 2282.

JEONG, J. & HUSSAIN, F. 1995 On the identification of a vortex. *Journal of Fluid Mechanics*, Vol. 285, 69.

LIU, X., Thomas, F. O. & Nelson, R. C. 2002 An experimental investigation of the turbulent planar wake in constant pressure gradient. *Physics of Fluids*, Vol. 14 (8), 2817.

NAKAYAMA, A. & LIU, B. The turbulent near wake of a flat plate at low Reynolds number. *Journal of Fluid Mechanics*, Vol. 217, 93.

RAI, M. M. 2010 A computational investigation of the instability of the detached shear layers in the wake of a circular cylinder. *Journal of Fluid Mechanics*, Volume 659, pp. 375-404.

RAI, M. M. 2011 Flow Physics and Self-Similarity in the Turbulent Near Wake of a Flat Plate. Paper 2011-3575, 41st AIAA Fluid Dynamics Conference, Honolulu, Hawaii.

RAI, M. M. 2013 Flow physics in the turbulent near wake of a flat plate. *Journal of Fluid Mechanics*, Volume 724, 704.

RAI, M. M. 2014 Flow Phenomena in the very near wake of a flat plate with a circular trailing edge. *Journal of Fluid Mechanics*, Volume 756, 510.

RAI, M. M. 2015 Detached shear-layer instability and entrainment in the wake of a flat plate with turbulent separating boundary layers. *Journal of Fluid Mechanics*, Volume 774, 5.

RAMAPRIYAN, B. R., PATEL, V. C. & SASTRY, M. S. 1982 The symmetric turbulent wake of a flat plate. *AIAA Journal*, Vol. 20 (9), 1228.

ROWE, A., FRY, A. L. A. & MOTALLEBI, F. 2001 Influence of boundary layer thickness on base pressure and vortex shedding frequency. *AIAA Journal*, Vol. 39 (4), 754.